Land Surface Temperature Detection in Relation to Land Use Land Cover Change: The Case of Jimma City and It's Surroundings, Jimma Zone, Southwest, Ethiopia

Nigus Tekleselassie Tsegaye (nigustselassie@gmail.com)
Ethiopian Environment and Forest Research institute; Hawasa Center https://orcid.org/0000-0002-8783-2955

Girma Alemu Melka
Jimma University College of Social Sciences and Law

Research

Keywords: Land Surface Temperature, LULC, NDVI, NDBI, Multiple linear regression

Posted Date: March 22nd, 2022

DOI: https://doi.org/10.21203/rs.3.rs-1388653/v1

Land Surface Temperature Detection in Relation to Land Use Land Cover Change: The Case of Jimma City and It's Surroundings, Jimma Zone, Southwest, Ethiopia

Nigus Tekleselassie TSEGAYE[1,*], Girma Alemu MELKA[2]

[1]Ethiopian Environment and Forest Research Institute, Tree seed technology research,

Hawasa Center

Phone: - +251924820727

P.O.Box:-1832,

Hawasa, Ethiopia

[2]Jimma University, CSSH, Department of Geography and Environmental Studies (GeES)

*Corresponding author: nigustselassie@gmail.com

Abstract

Introduction*:-Unmanaged land use and land cover change are major environmental issues that have a significant impact on the urbanization and agricultural development processes. The temperature of the land surface is rising as a result of this shift in land cover. The current study assesses the effect of changes in land use and land cover (LULC) on land surface temperature in Jimma and its surroundings. LULC, Normalized Difference Vegetation Index (NDVI), Normalized Difference Built-up Index (NDBI), and Land Surface Temperature (LST) were extracted from Landsat 5 TM (1987), Landsat 7 ETM$^+$ (2003), and Landsat 8 OLI/TIRS (2019) using digital image processing techniques. Change detection techniques were used to analyze LULC changes from 1987 to 2019. This study also analyzes the effect of NDVI and NDBI on LST between 1987 and 2019 with 368 sample points selected by stratified random sampling and using a multiple linear regression model.*

Result:- *The result showed that during the study period 1987-2019, agricultural land was the dominant land use which covered 54% of the study area. Settlement and agricultural land areas increased from 4.4% and 54.58% in 1987 to 12.27% and 62.40% in 2019 with the mean increase in land surface temperature from 20.53°C and 19.59°C to 33.60°C and 25.82°C, respectively. Forest cover, shrub land, water body, and wetland show decreasing trend. Correlation results of LST and NDBI have shown a strong positive relationship i.e. R^2 = 0.754 in 1987, 0.754 in 2003, and 0.739 in 2019, whereas strong negative correlations were found between LST and NDVI i.e. R^2 = 0.701, 0.737, and 0.746 in each year. The relationship between NDVI & NDBI was also developed and is showing a strong negative correlation i.e. R^2 = 0.739, 0.860, and 0.801.*

Conclusion:- *Hence, it was recommended that to reduce the land surface temperature, sustainable land use planning strategies that include increasing the vegetated areas and embracing other green initiatives such as the afforestation program should be adopted.*

Keywords*: Land Surface Temperature, LULC, NDVI, NDBI, Multiple linear regression*

1. Introduction

Due to human-induced activity, the earth's surface has been altered over thousands of years (Veldkamp & Lambin, 2001). High population pressure, migration, and rapid socioeconomic activity exacerbate these environmental changes (Zengin, *et al.,* 2018). Changes at diverse spatial scales, from local to global, have been discovered (Mahmood *et al.,* 2010). Agriculture and settlement expansion are two examples of large-scale human activities that are reducing the amount of vegetation on the earth's surface. As a result, carbon dioxide concentrations in the atmosphere are rising, influencing the surface energy budget and causing changes in local, regional, and global climate (Lilly R. & Devadas, 2009).

In many urban areas, population growth causes rapid urban expansion, resulting in changes in land use and land cover (LULC) (Coskun *et al.,* 2008). With rising population and rural-urban mobility, urbanization has risen throughout time, especially in developing countries. Developing countries, particularly those in Africa and Asia, are increasingly responsible for this fast urbanization (UN-Habitat, 2010). Specifically, between 2010 and 2015, urbanization in Africa is expected to increase by 56%, with an annual increase of 1.1%. Similarly, Ethiopia is one of the African countries whose urban dwellers have increased from 19% in 2014 and expected to be 38% in 2050. According to a UN (2014) study, Ethiopia's urban growth rate between 2010 and 2015 was 2.3%.

According to Sahoo (2013), increasing urbanization caused plenty of eco-environmental problems, such as a shift in land use and the rise of land surface temperature (LST). Urban growth combined with inappropriate land management methods has a significant influence on a city's local climate. The amount of solar radiation absorbed, evaporation rates, surface thermal storage, and wind turbulence are all affected by rapid land cover changes (Polydoros, *et al.,* 2018). Human exploitation of the natural environment via urban growth and expansion has a significant influence on the urban microclimate on a local and global scale. The increase in land surface temperature is one of the most significant effects of this extraction (Igun & Williams, 2018).

Changes in LULC have a significant impact on urban surface energy budgets (Alshaikh, 2015). It also resulted in a change in urban form and microclimate (Alqurashi & Kumar,

2013). The surface temperature has risen due to the transition of LULC classes to non-evaporating surfaces (Sahana *et al.,* 2016).

The need to thoroughly analyze the influence of LULC changes on the overall increase in the LST is becoming more important. Because various LULC surfaces or types emit and absorb energy radiation in different ways, they have been studied in order to determine LST (Pongratz, *et al.,* 2010). Estimating the cross-sectional relationship between LST and LULC types has also assisted researchers in investigating the impact of changing land cover on LST throughout time (Liu & Zhang, 2011). Several studies in cities have been undertaken to investigate the variability of the LST as a result of altering urban land cover types. Hu and Jia (2010) discovered that a decadal reduction in vegetation caused by changes in urban land cover in Guangzhou, southern China, resulted in an overall rise of 2.48 °C in LST between 1990 and 2007. A comparative study of Mumbai and Delhi revealed that the intensity of the UHI was greater in Mumbai than in Delhi due to changes in plant cover caused by urban development (Grover & Singh, 2015). The normalized difference vegetation index (NDVI) and the land surface temperature (LULC) were used to examine the land surface temperature in Bahir Dar. It has been found that converting LULC to urban landscaping increased LST. As a result, the maximum temperature in 1987 was 34.93 °C, while it reached 43.01 °C in 2017. This is an 8.08°C increase in LST (Balew, 2018). (Amiri *et al.,* 2009) discovered that surface temperature values change when travelling from a densely vegetated to a sparsely vegetated location. In most urban areas, tree cover or vegetation has been found to be inversely associated to LST (Raynolds *et al.,* 2008; Weng & Lu, 2008; Weng *et al.,* 2004). However, vegetation has long been believed to play an essential role in mitigating the effects of urban heating in urban contexts (Zhibin *et al.,* 2015; Chen *et al.,* 2013; Onishi *et al.,* 2010; Ali-Toudert & Mayer, 2007). But, accurately identifying hotspot regions inside current metropolitan areas, as well as incorporating green spaces into existing built-up areas, has proven difficult (Rotem-Mindali *et al.,* 2015).

As a result, tracking the trajectory of LULC change and its dynamism is critical in order to maintain global climate change (Aadil *et al.,* 2014). As a result, landscape analysis is a useful tool for tracking various LULC patterns and their variations (Arvor *et al.,* 2014).

Analyzing the effects of LULC changes on the Earth's surface, such as changes in and distributions of land surface temperature (LST), is also critical. Therefore, the main purpose of the study was to use geospatial technologies to assess the impact of changing forest cover on land surface temperature in Jimma and its surroundings between 1987 and 2019. Specific objectives of this study are: (1) To analyze the relationship between LST and land use and land cover change; (2) To examine the temporal and spatial change in LST as a function of LULC changes; and (3) To examine the effects of LULC changes on the research area's land surface temperature. This study was hypothesis that whether (1) there is no association between forest cover change and land surface temperature or there is an association between forest cover change and land surface temperature. (2) NDVI and NDBI variables have no significant effect on land surface temperature or NDVI and NDBI variables have a significant effect on land surface temperature in the study area.

2. Materials and Methods

2.1. Description of the study area

2.1.1. Location

The study area includes Jimma city and its surroundings, which is one of the oldest and historic cities in Ethiopia. It is found in in Jimma zone of Oromia National regional state, (Figure 1) and located 346 km to the Southwest of the Ethiopian capital, Addis Ababa. The geographical location of the study area extends from 7º 38' 0"N to 7º 46' 0"N latitude and 36º 42' 0"E to 36º 54' 0"E longitude. The study area has a total area of 24,915.13 ha, from which the terrestrial part was about 14,281.13 ha and 10,634 ha is the area of Jimma city.

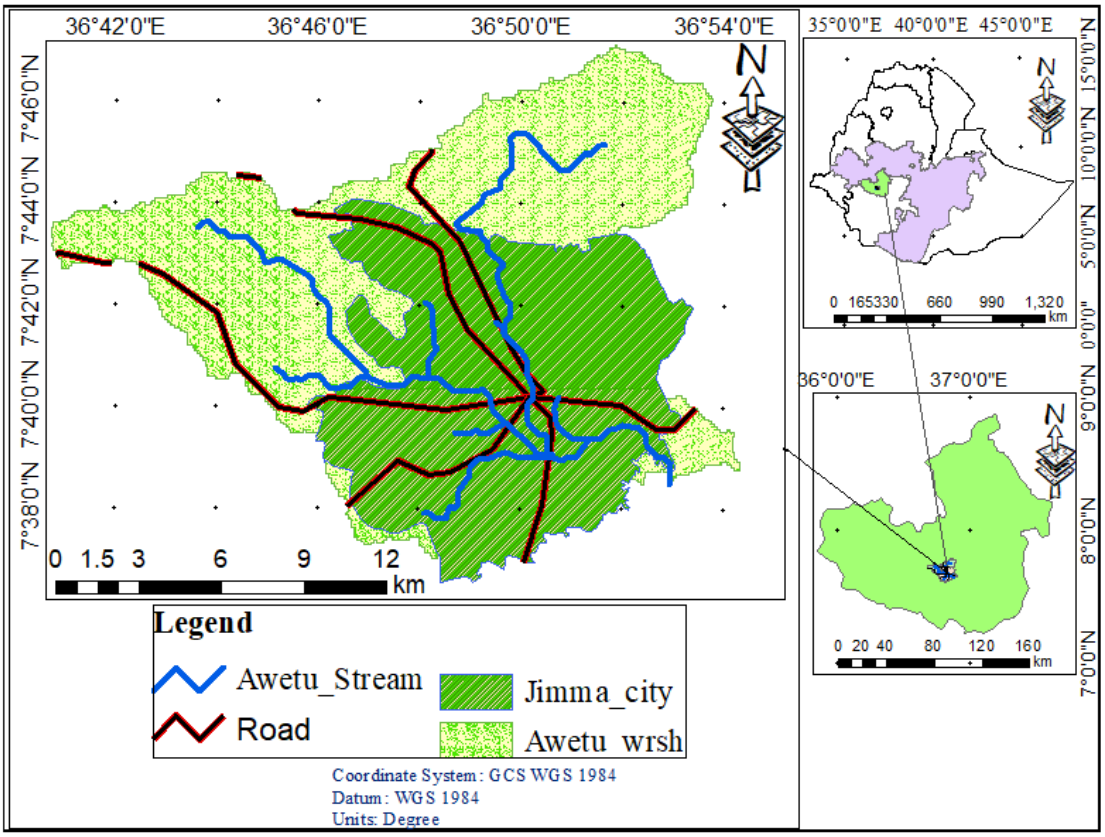

Figure 1: Locational Map of the Study area

Jimma city and its surroundings are located between a low point of 1676 meters above sea level in the south and a high point of 2581 meters above sea level in the west and east. The mean annual rainfall of the study area from 1987 to 2019 ranges from 913.3 mm to 2935.58 mm, according to thirty-two years of rainfall data obtained by the western Oromia region meteorological center (WORMC). During the 32-year study period, the mean annual rainfall varied from year to year, owing mostly to changes in climate and weather parameters. Despite the fact that Jimma and its surrounds receive virtually all of its precipitation year round, the highest annual rainfall recorded was in 1996, while the lowest annual rainfall record was in 2018. Agro climatically, the area is mainly woina dega type, accounting for around 47% of the entire area, while 35%, 35%, and 18% are in dega and kola zones, respectively (WORMC, 2019). The mean annual temperature of the study area is between 12^{o}C and 29^{o}C with a mean daily temperature of 19.5^{o}C. The maximum mean annual temperature of 26.26^{o}C in the study area was recorded in 2003 and the minimum mean annual temperature of 13.7^{o}C was recorded in 2007 (WORMC, 2019).

The Jimma city and its surrounds contain six primary soil classifications, according to FAO (2006) categorization. They are dystric nitisols (56.9%), eutricfluvisols (26.8%), dystric fluvisols (10.3%), chromic vertisols (3.6%), orthicacrisols (1.3%), and eutricnitisols (1.3%). (1.1%). At higher elevations, the soils are often reddish-brown and shallow, but at lower elevations, they tend to be gray and deep.

2.2. Design of the study

For the study, the causal research design was used since it attempted to reveal a cause-and-effect relationship between two variables. The LULC of the study area change matrixes was done quantitatively, followed by the LST of the study area generated from the Landsat image, and lastly the two findings were combined for relationship analysis.

The flow chart depicts the technique that was used in this study (Figure 2). It demonstrates the processes taken to extract the required information, beginning with the acquisition and classification of a multi-temporal satellite image of the study area. The initial stage was to analyze LULC information from Landsat 5, 7, and 8. LST estimate from Landsat imagery for the second step. Finally, correlation statistics for NDVI, NDBI, and LST were computed. Relationship analysis was performed for LULC and NDVI, as well as LULC and LST.

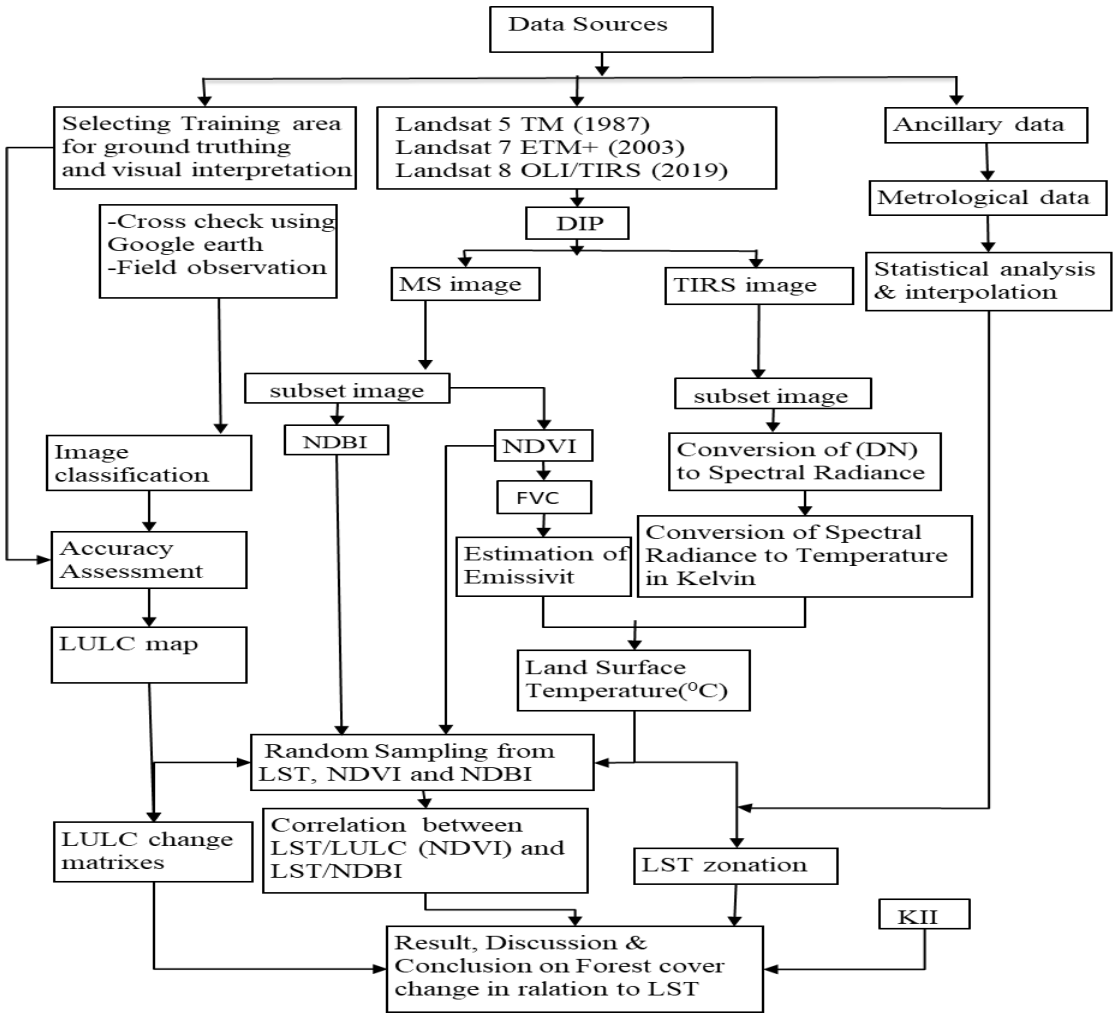

Figure 2: Methodological flow chart.

2.3. Data source and type

The study used both primary and secondary data sources to get the intended result.

I. **Primary data**: Unstructured key informant interviews and a field survey were used in the study. With the objective of establishing the underlying source of forest cover change and its influence on urban temperature, unstructured key informant interviews were conducted with nine elders from each sampled village. Field surveys were done using a Global Positioning System (GPS Garmin 72) to generate primary data for defining the research area's existing land-use type. The Google Earth map was used as a base map for image classification. It was also used to extract reference points for inaccessible locations as well as for the 1987 and 2003 images.

II. **Secondary data**: Different secondary data were used in the study to identify the land-use type, NDVI, NDBI, and analyze the land surface temperature of Jimma city and its surroundings. For this study, geospatial data and literature survey data from various sources were used. Digital geospatial datasets in raster forms collected from various sources for the preparation of factor maps, including: - The study area's Landsat images from 1987, 2003, and 2019 were used to analyze LULC change, NDVI, NDBI, and LST distribution.

During the study periods, meteorological data such as temperature and rainfall were used to describe the climate of the study area.

Many data for literature reviews were collected from the internet, while others were collected from books and reports, and all literature was categorized according to the research topic.

2.4.Meteorology Data

The Western Oromia region Meteorology Center provided meteorological data like as temperature and rainfall. The climate of the study area throughout the study periods was described using temperature and rainfall data.

2.5.Materials and tools

Arc GIS 10.4.1 software was used for image digitization, split and merge polygons, zonal statistics, reclassification, LST mapping, and mapping NDVI and NDBI. ERDAS IMAGINE 2015 software was used to process multi-temporal satellite images, which included image correction, enhancement, and processing (classification for LULC mapping and change calculation, LST calculation, and NDVI and NDBI generation). SPSS software was used to generate correlation statistics for LST, NDVI, and NDBI.

2.6.Methods of data collection

2.6.1. Remote sensing data

The three sets of remotely sensed data used for this study include: Landsat thematic mapper (TM), Enhanced thematic mapper (ETM+) and Landsat operational land imager (OLI), and Thermal infrared sensor (TIRS) images (with path/row 169/55) acquired during the month January 1987, February 2003, and January 2019 were used, because, these months were relatively free from cloud and haze. Due to the problem of poor resolution of MSS sensor

and data availability, the study period covered only from the year 1987 to 2019. Thus, the years 1987, 2003, and 2019 were selected for analysis with 16 years intervals. Detailed descriptions of Landsat datasets that were used for Landsat image sharpening, analyzing of LULC change, NDVI, NDBI, and LST distribution of Jimma city and its surroundings are given in Table 1.

Table 1: Description of data and their sources

Satellite	Sensors	Path & row	Resolution (m)	Acquisitions date	Source of data
Landsat	TM	169-055	30	01/31/1987	USGS
	ETM^{+}	169-055	30	02/20/2003	"
	OLI	169-055	30	01/23/2019	"
Thermal Infrared (band 10)	TIRS	169-055	100	01/23/2019	"
Thermal Infrared (band 11)	TIRS	169-055	100	01/23/2019	"
DEM			12.5 (m)	2019	ASF

2.6.2. Ground Truth Data

In the study area, a stratified random sample technique was employed to perform a ground truth activity in which various LULC classes were validated. Agriculture, forest cover, settlement, shrub land, wetland, and water body were evaluated in the observed LULC from largest to smallest. The map legends were generated using these LULC classes, and the training data set for image classification was obtained using GPS. Furthermore, accuracy was measured using ground truth data. During these ground-truth activities, photos of areas of interest and coordinates from sampling LULC classes were collected.

2.7.Methods of data analysis

2.7.1. Digital image preprocessing

Landsat images were obtained from the USGS database for 1987, 2003, and 2019 using the Thematic Mapper (TM), Enhanced Thematic Mapper (ETM+), operational land imager (OLI), and thermal infrared sensor (TIRS). Each image was geometrically and radiometrically adjusted as in (Orimoloye, *et al.,* 2018). For the purpose of LULC classification image analysis, the spectral bands were layer stacked to produce a composite

image of the study area for each year (1987, 2003, and 2019). Thermal band 6 for Landsat 5 TM, ETM+, and bands 10 & 11 for Landsat 8 TIRS were used to calculate LST from all time periods. Thermal bands originally had pixel sizes of 120 m for TM and 100 m for TIRS images, which were resampled to 30 m using the nearest-neighbor algorithm to match the pixel size of other spectral bands. A land cover classification was necessary for the detection of LULC changes as a result of fast urbanization from 1987 to 2019 in order to examine the effects of human activities in the study area. Following the selection of training areas, the Landsat images were classified using bands 2 (green), 3 (red), and 4 (near-infrared) via supervised classification using the maximum-likelihood algorithm . Visual image interpretation was performed using field knowledge and Google Earth images of the study area. The error matrix of the three LULC maps were generated to evaluate the classification result's accuracy. The projection transformation was performed and assigned to the WGS 1984 UTM Zone 37 N projection to make the data compatible with each other.

2.7.2. Image classification

Image classification is the task of extracting information classes from a multiband (multi-spectral) raster image or extracting information based on the reflectance of an object, and it serves particular purposes, such as converting image data into thematic data (Gao, 2009; Richards & Jia, 2006). The information class can be grouped into a thematic layer of LULC in the image that have similar LULC. Despite the availability of automatic image classification techniques, a human or visual image interpretation approach was employed. This is due to a pixel mixing issue, particularly in low-resolution imageries like Landsat, which has significantly affected the study's LULC classification accuracy.

To obtain the LULC of the study area, ERDAS imagine used a supervised classification method. The maximum likelihood algorithm was used for supervised classification among different classification techniques by taking the ground control points for six major LULC class categories.

2.7.3. Accuracy assessment

The comparison of image interpretation by a computer using ground truth data is known as accuracy assessment (Gao, 2009; Richards & Jia, 2006). The training sites utilized in this comparison for accuracy evaluation were selected using a stratified random sampling method. Stratified sampling classifies groups based on the similarity of spectral features.

To ensure that minor but important land covers are included in the sample, stratified random sampling is required. Stratified random sampling is required to ensure that minor but important land covers are included in the sample (Russell, *et al.,* 2019). Each LULC category has its own stratum. A sample of LULC classification was obtained by clustering many training pixels in the feature space. As specified by the operator, the clusters should constitute a representative data set for a specific class. The number of sample plots (clusters, with one cluster having a sample size of 30 n, where n is the number of bands) (Wim, *et al.,* 2004). Although some adjustments were made during the fieldwork to account for physical obstacles and other variables, the number of samples was calculated based on the area percentage. The sample unit had a radius of 20 meters and was part of a cluster of six sample units, including the center, 200 meters apart. For the 1987, 2003, and 2019 LULC classifications, 210 points were randomly collected from the study area, which is 30 times the number of bands (7).

Overall accuracy was used to calculate a measure of accuracy for the entire image across all classes present in the classified image (Eq. 1). The collective accuracy of a map for all the classes can be described using overall accuracy, which calculates the proportion of pixels correctly classified.

$$Overall\ Accuracy = \frac{\text{Sum of the diagonal elements}}{\text{Total number of accuracy sites pixels (column total)}} \qquad \text{Eq.1}$$

Congalton (1991) presented the Kappa coefficient (K) as an additional assessment that may be used in this study in addition to overall accuracy. The K technique is computed by increasing the total number of pixels in all the ground verification classes (N) with the sum of the confusion matrix diagonals (X_{ii}) and subtracting the sum of the ground verification pixels during the class time. The sum of the classified pixels in that class is summed up over all classes ($\Sigma X_i \Sigma\ X_I$), where ΣX_i is the row total and ΣX_I is the column total, and divided by the total number of pixels squared minus the sum of the ground verification pixels in that class times the sum of the classified pixels in that class summed over the classes.

$$k = \frac{N \sum_{i=1}^{k} x_{ii} - \sum_{i-1}^{k} (x_i * x_I)}{N^2 - \sum_{i-1}^{k} (x_i * x_I)} \qquad \text{Eq.2}$$

$$k = \frac{(Total\ Sum\ of\ correct) - Sum\ of\ the\ all\ (row\ total\ column\ total)}{\text{Total squared} - \text{Sum of the all (row total column total)}} \quad \text{Eq.3}$$

In general, the Kappa Coefficient is generated from a statistical test to evaluate the accuracy of classification. Kappa essentially evaluates how well the classification performed as compared to just randomly assigning values, i.e. did the classification do better than random. The Kappa Coefficient can range from -1 to 1. A value of 0 indicated that the classification is no better than a random classification. A negative number indicates the classification is significantly worse than random. A value close to 1 indicates that the classification is significantly better than random.

2.7.4. Land use land cover thematic layer

After classification accuracy was conducted, final LULC were identified and mapped for the three study periods (that is, 1987, 2003, and 2019). So, Jimma city and its surroundings have the following LULC classes.

Table 2: LULC classes and description of the study area

No.	LULC Classes	Description
1	Agricultural land	Areas of land plowed/prepared for growing rain-fed crops. It also includes land with scattered or patches of trees and it is used for grazing and browsing of domestic animals and Areas of land prepared for growing crops.
2	Forest Cover	It represents both natural and fragmented plantation forest areas that are stocked with trees capable of producing timber or other wood products
3	Settlement	The area occupied by house buildings includes road network residential, commercial and industrial, transportation, roads, and mixed urban and other facilities.
4	Shrubland	land supporting an assemblage of small trees and shrubs
5	Wetland	A land area that is saturated with water
6	Waterbody	Areas covered by natural and manmade small dams, like pond and river

2.7.5. Change detection

A change detection analysis was carried to assess the rate of increase or decrease in the LST over smaller areas. A statistical approach was used to carry a correlation and regression study to show the relationship between the LST and the various land cover types. This was done by calculating the percentage proportion of land cover categories and their mean LST in 1987, 2003, and 2019, respectively. Vegetated and non-vegetated areas were classified into percentage proportions of land cover types. This is due to the fact that classifying land cover types into vegetated and non-vegetated areas aids in estimating the relationship between the LST and the various land cover types. To analyze how the total area of LULC changed from 1987 to 2019, the initial and final LULC area coverage were computed following Garai & Narayana (2018) as indicated in Eq.4.

$$Rate\ of\ LULC\ change = \frac{(Present\ LULC\ area - Previous\ LULC\ area)}{Previous\ LULC\ area} x100 \quad \text{Eq.4}$$

2.7.6. Multispectral radiometric correction

Radiometric correction necessitates the conversion of a remote sensing digital number to spectral radiance values and data for comparison. Image processing techniques used to correct errors, such as converting digital number (DN) values to spectral radiance and subsequently reflectance, were categorized as radiometric corrections (Prata & Caselles, 1995). To convert a digital number to a spectral radiance, equation (5) was utilized in ERDAS IMAGINE using the USGS formula (2019).

$$L_\lambda = M_\lambda * Q_{cal} + A_L \quad \text{Eq.5}$$

Where; L_λ = Spectral radiance (W/ (m^2 * sr * μm)); M_λ= Radiance multiplicative scaling factor for the band (RADIANCE_MULT_BAND_N from the metadata); AL = Radiance additive scaling factor for the band (RADIANCE_ADD_BAND_N from the metadata); Q_{cal} = Level 1 pixel value in DN.

2.7.7. Thermal atmospheric correction

In radiometric calibration, pixel values, which were represented by Q in remote sensing raw data and unprocessed image data, were changed into absolute radiance values. Hence, the spectral radiance of TM, ETM+, and OLI images was converted into radiance using the equation (NASA, 2000).

$$L\lambda = \left(\frac{LMAX\lambda - LMIN\lambda}{QCALMAX - QCALMIN}\right)(QCAL - QCALMIN) + LMIN\lambda \quad \text{Eq.6}$$

Where: L_λ = Spectral radiance received by the sensor (W/ (m^2 * sr * μm))

QCAL = the quantized calibrated pixel value in DN

$LMIN_\lambda$ = the spectral radiance that is scaled to QCALMIN (W/ (m^2 * sr * μm))

$LMAX_\lambda$ = the spectral radiance that is scaled to QCALMAX (W/ (m^2 * sr * μm))

QCALMIN = the minimum quantized calibrated pixel value (corresponding to $LMIN_\lambda$ in DN which is 1

QCALMAX = the maximum quantized calibrated pixel value (corresponding to $LMAX_\lambda$ in DN which is 255

2.7.8. Conversion of radiance into brightness temperature

After spectral radiance was converted to radiance, the raw digital numbers of the thermal bands are converted to at-satellite brightness temperatures, which were the effective temperature viewed by the satellite under an assumption of uniform emissivity (Rajeshwari & Mani, 2014).

$$BT = \frac{K2}{\ln(\frac{K1}{L\lambda}+1)} \quad \text{Eq.7}$$

Where; BT = effective at-sensor brightness temperature in Kelvin

$K1$ = calibration constant 1 (W/ (m^2 * sr * μm))

$K2$ = calibration constant 2 (W/ (m^2 * sr * μm))

$L\lambda$ = spectral radiance at the sensor's aperture (W/ (m^2 * sr * μm))

ln = natural logarithm

The temperature values estimated using Eq.9 were converted from Kelvin (K) to Celsius (^oC) (a standard unit of measuring temperature) by subtracting 273.15.

Table 3: Thermal constants of Landsat images

Satellite	sensors	Categories	Band 6	Band 10	Band 11
Landsat 5	TM	K1	607.76		
		K2	1260.56		
Landsat 7	ETM+	K1	666.09		
		K2	1282.71		
Landsat 8	OLI/TIRS	K1		774.8853	480.8883
		K2		1321.0789	1201.1442

2.7.9. Normalized difference vegetation index

Eq. 7 was used to calculate the Normalized Difference Vegetation Indices for the study area for 1987, 2003, and 2019. In the near-infrared part of the spectrum, vegetated areas reflect better (Roberts, *et al.,* 2015). The normalized difference vegetation index is also used to predict general vegetation conditions and calculate the LST. The red band (high absorption of radiation or low reflection) and the infrared band (low absorption of radiation or high reflection) were used to calculate the NDVI. Green leaves have a reflectance of 20% or less in the 0.5 to 0.7-micrometer range and about 60% in the 0.7 to 1.3 range (Farooq, *et al.,* 2013). Therefore, NDVI values represent ratios ranging in value from −1.0 to 1.0. Accordingly, NDVI can be computed as

$$NDVI = \frac{\text{NIR}-\text{RED}}{NIR+RED} \qquad \text{Eq.8}$$

NDVI=Normalized Difference Vegetation Index

NIR= near-infrared band 4, RED= is the red band 3. The equation was used to calculate NDVI for the sensor TM, $ETM^{+,}$ and OLI. But in the case of Landsat 8, NIR is band 5 and the red band is a band 4 (Weng, *et al.,* 2004).

2.7.10. Normalized difference built-up index

NDBI stands for Normalized Difference Built-up Index, In comparison to the other LULC surfaces, built-up lands have higher reflectance in the MIR wavelength range (1.55~ 1.75μm) than in the NIR wavelength range (0.76~ 0.90μm) (John & David, 1999). NDBI is very useful for mapping the urban built-up areas and has been computed using the equation (8) expressed as follows;

$$NDBI = \frac{MIR-NIR}{MIR+NIR} \qquad \text{Eq. 9}$$

Where *NIR* is near-infrared reflectance

MIR is middle infrared reflectance

NDBI values range from -1 to 1. The greater the NDBI is, the higher the proportion of built-up land is, and the larger areas of construction land have.

2.7.11. Land surface emissivity

To estimate LST the land surface emissivity (LSE (ε)) must be known because LSE is a proportional factor that scales blackbody radiance (Planck's law) to predict emitted radiance. In satellite images, pixels representing the land surface are usually mixed pixels, that is, they are a combination of surfaces-types such as water, vegetation, and soil. Therefore, the effective emissivity of a pixel can be calculated by summing up the contributions from those surface types because the emissivity value change from surface to surface. Though to estimate the emissivity from satellite thermal band data quite a lot of methods have been suggested, the NDVI threshold method was used in this study. Land surface emissivity was calculated via the following formula.

$$\varepsilon_\lambda = \varepsilon_v F_v + \varepsilon_s (1 - F_v) + (1 - \varepsilon_s)(1 - \varepsilon_v) F \varepsilon_v \quad \text{Eq. 10}$$

Where ε_v and ε_s are the vegetation and soil emissivity, respectively, F = 0.55 shape factor considering different geometrical distributions, the fractional vegetation, F_v, was determined using the following equation (Meijun *et al.,* 2015).

$$F_v = \left(\frac{NDVI - NDVI_{min}}{NDVI_{max} - NDVI_{min}}\right)^2 \quad \text{Eq.11}$$

2.7.12. Statistical Analysis

To determine the correlations for each pixel, Pearson's correlation coefficients were calculated between the LST and the corresponding LULC indices values. Randomly, 368 points have been extracted from the image through ArcGIS software, finding the corresponding values of LST, NDVI, and NDBI for each year to estimate the relationship between them. The values were statistically analyzed for the creation of a model using multiple linear regression with the help of Statistical Package for the Social Sciences (SPSS) version 20.

$$Y = \beta 0 + \beta 1 X1 + \beta 2 X2 + \beta 3 X3 + \ldots\ldots + \beta n Xn \quad \text{Eq. (12)}$$

Where: Y= the dependent variable (LST)

β0 =Constant term of the model without the independent variables;

β1, β2...β10 = The Estimated influences of the specified independent variables;

X1, X2, to X10 = Independent variables which would be the predictor of the dependent variable

ANOVA and t-test were also applied to assess statistical significance between LST, NDVI, and NDBI. The relationship between land surface temperature and NDVI and NDBI can be determined by passing a multiple linear regression test. In the multiple linear regression test, the land surface temperature is taken as a dependent variable, while NDVI and NDBI are taken as independent variables for predicting the land surface temperature.

3. Results and Discussions

3.1. Results

3.1.1. LULC classes in 1987

The spatial extent of the 1987 LULC map after the Supervised Classification yielded land cover classes (Figures 3 and Table 4) with the high-density agriculture occupying the highest percentage of the area (13597.6 ha, 54.58%). The next LULC class with the highest area coverage was the forest (5087.52 ha, 20.42%) which was scattered around the North, South-West, South-East, and Western parts of the study area with very small patches in the southern part. Shrub land (3714.69 ha, 14.91%) was the next highest LULC class in the study area. Wetland comes next with (1389.65 ha, 5.58%) which was located around the south and South-Western part of Jimma city. This is followed by the settlement (1096.87 ha, 4.40%) located mainly around the center of the study area and water body (28.8 ha, 0.12%) was last and the least area coverage and concentrated in the eastern part of Jimma city.

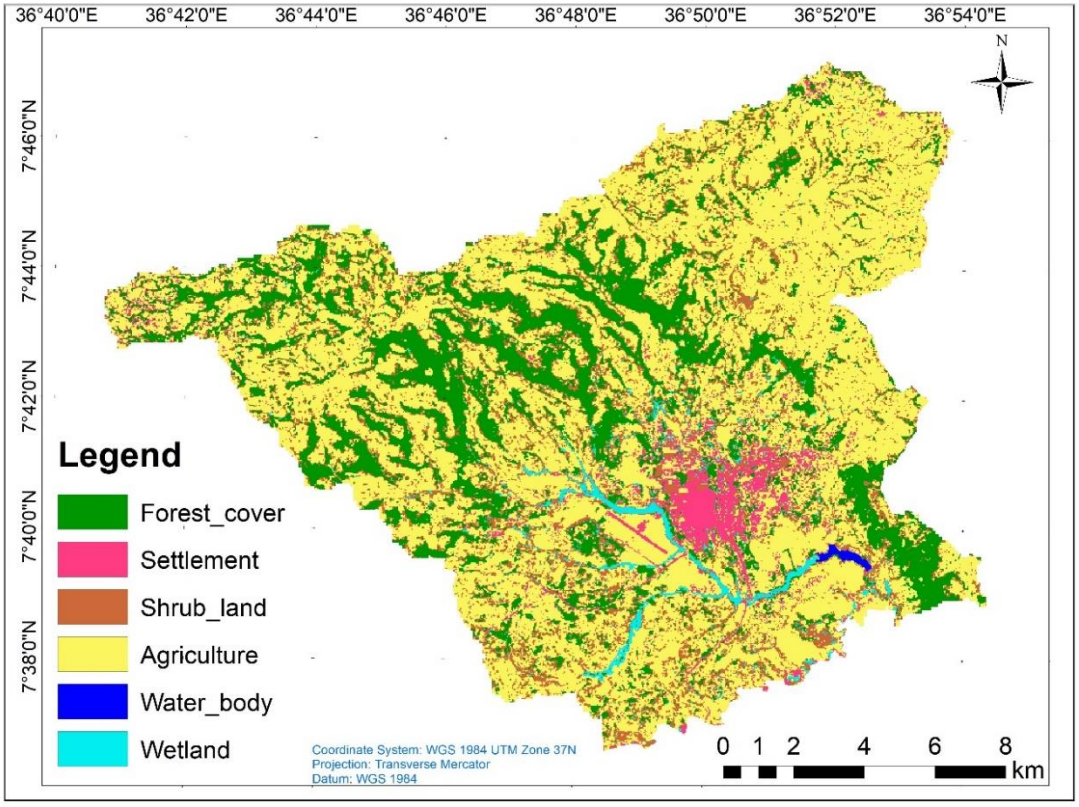

Figure 3: LULC map of the study area in 1987

Source: 1987 satellite image interpretation

Table 4: LULC classes and their area coverage in the three periods.

LULC classes	1987		2003		2019	
	ha	%	ha	%	ha	%
FC	5087.52	20.42	3293.54	13.22	3858.23	15.49
SET	1096.87	4.40	1881.04	7.55	3057.09	12.27
SH	3714.69	14.91	2615.4	10.50	1624.88	6.52
AG	13597.6	54.58	15836.1	63.56	15546.44	62.40
WB	28.8	0.12	16.56	0.07	0	0.00
WE	1389.65	5.58	1272.49	5.11	828.49	3.33
Total	24915.13		24915.13		24915.13	

Where: FC= Forest cover, SET= Settlement, SH= Shrub land, AG= Agriculture, WB= Water body and WE= Wetland.

3.1.2. LULC classes in 2003

The Supervised classification procedures applied to the 2003 Landsat ETM+ image yielded a land cover map with the high-density agriculture occupying the largest area coverage of (15836.1ha, 63.56%) as compared to other LULC classes (Figures 4 and Table 4). Forest covers an area of (3293.54ha, 13.22%) and is scattered around the North, South-West, South-East, and Western parts of the study area. Shrub land (3714.69 ha, 14.91%) was the third-highest LULC class in the study area. The settlement occupies an area of (1881.04ha, 7.55%) and is mainly concentrated at the center parts of the map. Wetland comes next with (1272.49ha, 5.11%) which was located around the southern part of Jimma city. Water body having (16.56ha, 0.07%) was the least area coverage and mainly concentrated in the eastern part of Jimma city.

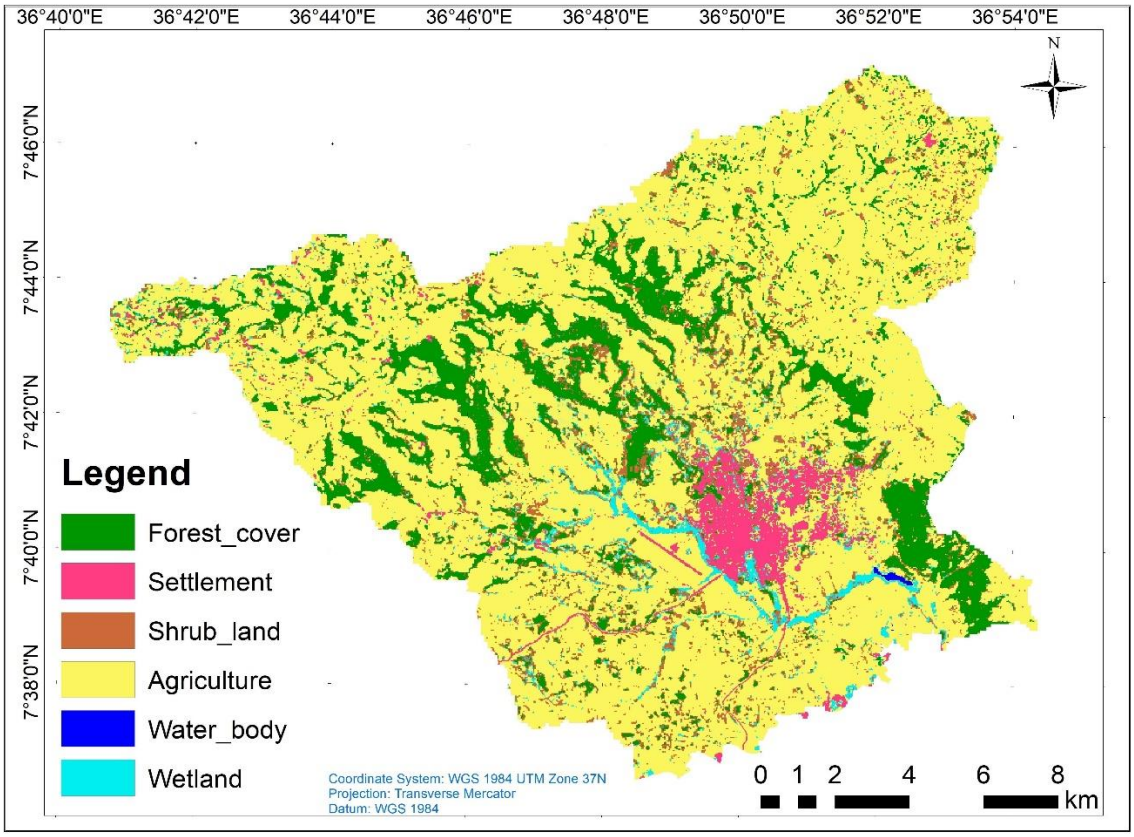

Figure 4: LULC map of the study area in 2003

Source: 2003 satellite image interpretation

3.1.3. LULC classes in 2019

The 2019 Landsat OLI/TIRS after classification procedures yielded a Land cover map with the high-density agriculture occupying an area of (15546.44ha, 62.40%). Forest covers an area of (3858.23ha, 15.49%) and mainly around the North, South-West, South-East, and Western parts of the study area with very small patches in the southern part. The settlement occupies an area of (3057.09ha, 12.27%). This was concentrated at the center of the map and small patches at the entire map. As (Figures 5 and Table 4) shows that shrub land, wetland, and water body have a dramatic decline and they account (1624.88ha, 6.52%), (828.49ha, 3.33%), and (0ha, 0.00%) respectively.

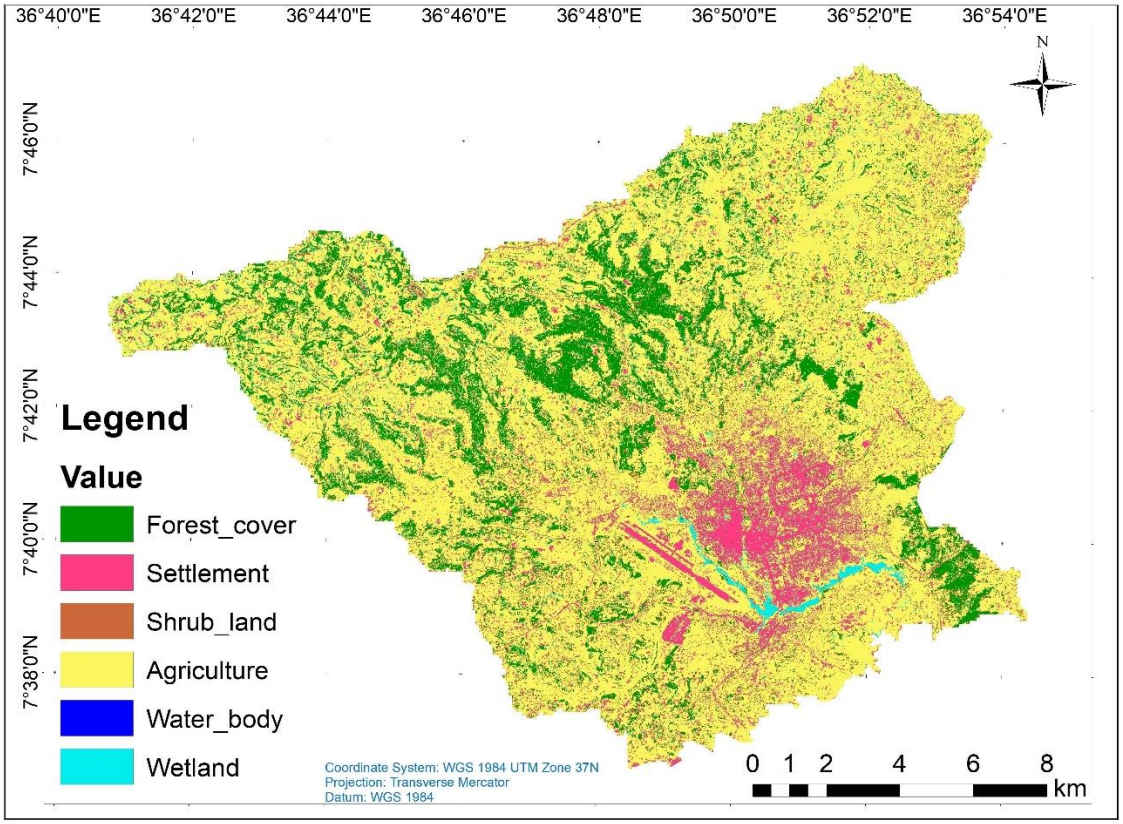

Figure 5: LULC map of the study area in 2019

Source: 2019 satellite image interpretation

3.1.4. LULC change between 1987 to 2003

The analysis of LULCC revealed that the agricultural land was 13597.6 ha (54.58%) of the study area in 1987 was increased to 15836.1ha (63.56%) in 2003 (Table 5). The net change in agricultural land was (14.14%, a positive rate of change). The settlement land was experienced the most positive change 41.69%, while water body experienced the most negative change (-73.91%). In contrary to settlement and agricultural land areas, forest cover, shrub land, and wetland areas were experienced negative change with (-54.47%), (-42.03), and (-9.21%) respectively (Figure 10).

Table 5: Extent of LULC change in 1987 and 2003 years.

LULC classes	1987		2003		Net-Change
	ha	%	ha	%	1987-2003 (%)
FC	5087.52	20.42	3293.54	13.22	-54.47
SET	1096.87	4.40	1881.04	7.55	41.69
SH	3714.69	14.91	2615.4	10.50	-42.03
AG	13597.6	54.58	15836.1	63.56	14.14
WB	28.8	0.12	16.56	0.07	-73.91
WE	1389.65	5.58	1272.49	5.11	-9.21
Total	24915.13		24915.13		

Where: FC= Forest cover, SET= Settlement, SH= Shrub land, AG= Agriculture, WB= Water body and WE= Wetland.

3.1.5. LULC change between 2003 to 2019

When analyzing the 2003 LULC classification with the 2019 LULC classification, the forest cover class shows increasing in the study area from 2003 to 2019 (Table 6). The increment of forest LULC was a direct reflection of the government policy of the millennium afforestation program to enhance the forest coverage of the country. The settlement land cover class shows a remarkable increase between 2003 and 2019, which has been increased in size from 1881.04 ha in 2003 to 3057.09 ha in 2019 with a net change (38.47%, positive rate of change), while the water bodies were experiencing an extremely decreased from 16.65 ha in 2003 to 0 ha in 2019. The increment of settlement area over

the study period was associated with rapid population growth, migration of people from a neighboring city, and unable to compete for the land lease price. These results are consistent with (Mosammam *et al.,* 2017) who reported that the rapid urban population is a key challenge of the twenty-first century. Two land cover classes namely settlement and agricultural land show an increasing trend throughout the study periods (Table 6).

Table 6: Extent of LULC change in 2003 and 2019 years.

LULC classes	2003		2019		Net-Change
	ha	%	ha	%	2003-2019 (%)
FC	3293.54	13.22	3858.23	15.49	14.64
SET	1881.04	7.55	3057.09	12.27	38.47
SH	2615.4	10.50	1624.88	6.52	-60.96
AG	15836.1	63.56	15546.44	62.40	-1.86
WB	16.56	0.07	0	0.00	0.00
WE	1272.49	5.11	828.49	3.33	-53.59
Total	24915.13		24915.13		

Where: FC= Forest cover, SET= Settlement, SH= Shrub land, AG= Agriculture, WB= Water body and WE= Wetland.

3.1.6. LULC change between 1987 to 2019

Generally, the trend analysis of the study area reveals a change in the LULC types over the three study periods (Table 7). The settlement experienced the most positive change 64.12%, while shrub land experienced the most negative change (-128.61%) during the years 1987 to 2019. The settlement land increased from 1987 to 2019 covering an area of 1096.87ha (4.40%) in the year 1987 and 1881.04 ha (7.55%) in the year 2003 and 16 years later this land cover class increased to 3057.09 ha (12.27%) in the year 2019. The study conducted by (Dube, 2013) also found comparable results with increased settlement areas due to rapid, unstructured, and unplanned development. The increasing trends are also observed in agricultural land. However, the shrub land and forest cover that occupies over 3714.69 ha (14.91%) and 5087.52 ha (20.426%) in 1987 respectively, decreased to 1624.88 ha (6.52%) and 3858.23 ha (15.49%) in 2019 respectively.

Table 7: Extent of LULC change in 1987 and 2019 years.

LULC classes	1987		2019		Net-Change
	ha	%	ha	%	1987-2019 (%)
FC	5087.52	20.42	3858.23	15.49	-31.86
SET	1096.87	4.40	3057.09	12.27	64.12
SH	3714.69	14.91	1624.88	6.52	-128.61
AG	13597.6	54.58	15546.44	62.40	12.54
WB	28.8	0.12	0	0.00	0.00
WE	1389.65	5.58	828.49	3.33	-67.73
Total	24915.13		24915.13		

Where: FC= Forest cover, SET= Settlement, SH= Shrub land, AG= Agriculture, WB= Water body and WE= Wetland.

The declining trend of the shrub land and forest cover was due to increasing land requirements for house construction and arable land, which arising from (rapid population growth, density, and internal migration), urbanization, and uncontrolled response by the government (Deribew & Dalacho, 2019), which enhances the problem of informal house constructions. These findings are supported by (Abebe *et al.,* 2019), who reported urban informality, is the outcome of either the population who lives in substandard living conditions or a housing deficit. It is observed that the water body has decreased from 28.8 ha (0.12%) in the year 1987 to 16.56 ha (0.07%) in the year 2003, and the decreasing trend of water body was continued throughout the study period and decreased to 0 ha (0%) by the year 2019. The wetland of the study area also shows a decreasing trend from 1987 to 2019 covering a total area of 1389.65 ha (5.58%) in the year 1987 and 828.49 ha (3.33%) in 2019. The decreasing trend in both water bodies and wetland is because the deposition of sediment in the water bodies and wetland resulted, silt from farmland, sludge from infrastructure built in the city, and housing. In agreement with the finding of this study (Abrha *et al.,* 2015) also reported the reduction of water bodies and wetland between 1984 and 2007 were corresponding to the drastic consequences of ever-increasing demand for residential and institutional building construction spaces in Jimma city.

3.2. Land use land cover change matrix

To acquire changes of the six LULC classes over the study period (1987–2019), the change matrix was conducted through cross-tabulation to investigate the trend, net change, and percent change between 1987 and 2003, 2003 and 2019, and for the overall study period 1987 and 2019.

Table 8 shows a summary of the major LULC conversions that have been taken place from 1987 to 2003 within the study area. The diagonal of the table shows the LULC proportions that remain unchanged from 1987 to 2003, a total area of 19,130.5 ha representing 76.78% of the study area. From the table, forest cover in 1987 was converted into agricultural land, shrub land, and settlement in 2003. The major forest cover transformation made by the expansion of agricultural land was (22.05%) and shrub land was (12.70%). In contrary to this, (0.99%) Forest cover was gained from shrub land in 2003. Shrub land also changed to agricultural land, wetland, and settlement in 2003. Furthermore, the water body was transformed into wetland, agriculture, shrub land, and settlement. Similarly, the wetland was changed to agriculture, shrub land, and settlement in 2003. Details about the LULC transformation matrix from 1987-2003 are illustrated in Table 8.

Table 8: LULC changes matrix of the Jimma city and its surrounding from 1987 to 2003 (ha)

		LULC of 2003													
	LULC	FC		SET		SH		AG		WB		WE		class total	
	Class	ha	%	ha	%	ha	%	ha	%	ha	%	ha	%	ha	%
LULC of 1987	FC	3199.06	62.88	120.29	2.36	646.05	12.70	1121.75	22.05	0	0.00	0.37	0.01	5087.52	100
	SET	0.64	0.06	1030.32	93.93	21.37	1.95	44.54	4.06	0	0.00	0	0.00	1096.87	100
	SH	36.81	0.99	133.77	3.60	1766.1	47.54	1595.87	42.96	0	0.00	182.14	4.90	3714.69	100
	AG	51.94	0.38	582.04	4.28	94.09	0.69	12452.92	91.58	0	0.00	416.61	3.06	13597.6	100
	WB	0	0.00	0.45	1.56	0.54	1.88	3.42	11.88	16.56	57.50	7.83	27.19	28.8	100
	WE	5.09	0.37	14.17	1.02	87.25	6.28	617.6	44.44	0	0.00	665.54	47.89	1389.65	100
	class total	3293.54	13.22	1881.04	7.55	2615.4	10.50	15836.1	63.56	16.56	0.07	1272.49	5.11	24915.13	100

Where: FC= Forest cover, SET= Settlement, SH= Shrub land, AG= Agriculture, WB= Water body and WE= Wetland.

As Table 9 shows, from the total area of forest cover in 2003, 785.01 ha (23.83%), 254.32 ha (7.72%), and 48.24 ha (1.46%) were converted to agriculture, shrub land, and settlement in 2019, respectively. On contrary, forest cover was gained from shrub land 845.79 ha and agricultural land 804.97 ha in 2019. During 2003-2019, shrub land was also converted into agriculture and settlement. The conversion of agricultural land to other LULC classes such as settlement (6.38%), shrub land (4.32%), and wetland (2.44%) after sixteen years. Water body also changed into wetland (55.31%), agriculture (42.81%), shrub land (1.03%), and settlement (0.87%) in the year 2019. Similarly, the wetland was transformed into agriculture, shrub land, and settlement. Table 9 present the detailed information of LULC transformation from 2003 to 2019.

Table 9: LULC changes matrix of the Jimma city and its surrounding from 2003 to 2019 (ha)

		LULC of 2019													
	LULC	FC		SET		SH		AG		WB		WE		class total	
	Class	ha	%	ha	%	ha	%	ha	%	ha	%	ha	%	ha	%
LULC of 2003	FC	2205.94	66.98	48.24	1.46	254.32	7.72	785.01	23.83	0	0.00	0.03	0.00	3293.54	100
	SET	1.5	0.08	1831.21	97.35	9.32	0.50	39.01	2.07	0	0.00	0	0.00	1881.04	100
	SH	845.79	32.34	113.41	4.34	568.79	21.75	1081.9	41.37	0	0.00	5.51	0.21	2615.4	100
	AG	804.97	5.08	1010.27	6.38	683.84	4.32	12950.89	81.78	0	0.00	386.13	2.44	15836.1	100
	WB	0	0.00	0.14	0.85	0.17	1.03	7.09	42.81	0	0.00	9.16	55.31	16.56	100
	WE	0.03	0.00	53.82	4.23	108.44	8.52	682.54	53.64	0	0.00	427.66	33.61	1272.49	100
	class total	3858.23	15.49	3057.09	12.27	1624.88	6.52	15546.44	62.40	0	0.00	828.49	3.33	24915.13	100

Where: FC= Forest cover, SET= Settlement, SH= Shrub land, AG= Agriculture, WB= Water body and WE= Wetland.

While considering the whole range of time under consideration, the reduction in the area covered by forest, shrub land, water body, and wetland were observed. Image differencing of the two different times, 1987, and 2019 indicated that forest cover was reduced from 5087.52 ha to 3858.53 ha (1229.29 ha) representing 31.86% of the area. The conversion of forest cover to other LULC classes such as agriculture (39.15%), shrub land (9.11%), and settlement (3.50%). On contrary, forest cover was gained from shrub land (13.89%) and agricultural land (6.43%). Other LULC conversions are shrub land to agricultural land (64.85%), settlement (6.96%), and wetland (2.03%). Agricultural land was also transformed into settlement (10.85%) and shrub land (4.96%). Furthermore, water body was changed to wetland (54.51%), agricultural land (42.95%), and shrub land (2.05%). Similarly, the wetland was also changed to agriculture (45.79%), settlement (5.78%), and shrub land (1.71%). The LULCC matrix of the study area from 1987 to 2019 is illustrated in (Table 10).

Table 10: LULC changes matrix of the Jimma city and its surrounding from 1987 to 2019 (ha)

		LULC of 2019													
	LULC	FC		SET		SH		AG		WB		WE		class total	
	Class	ha	%	ha	%	ha	%	ha	%	ha	%	ha	%	ha	%
LULC of 1987	FC	2453.73	48.23	178.16	3.50	463.46	9.11	1991.54	39.15	0	0.00	0.63	0.01	5087.52	100
	SET	7.5	0.68	1065.25	97.12	6.45	0.59	17.67	1.61	0	0.00	0	0.00	1096.87	100
	SH	515.84	13.89	258.49	6.96	455.72	12.27	2409.1	64.85	0	0.00	75.54	2.03	3714.69	100
	AG	874.51	6.43	1474.79	10.85	674.95	4.96	10479.11	77.07	0	0.00	94.24	0.69	13597.6	100
	WB	0	0.00	0.14	0.49	0.59	2.05	12.37	42.95	0	0.00	15.7	54.51	28.8	100
	WE	6.95	0.50	80.26	5.78	23.71	1.71	636.35	45.79	0	0.00	642.38	46.23	1389.65	100
	class total	3858.53	15.49	3057.09	12.27	1624.88	6.52	15546.14	62.4	0	0.00	828.49	3.33	24915.13	100

Where: FC= Forest cover, SET= Settlement, SH= Shrub land, AG= Agriculture, WB= Water body and WE= Wetland.

3.3. Accuracy Assessment

The accuracy evaluation of LULC for the year 2019 was validated using a ground-truth assessment of 210 sample GPS points taken from the study area, resulting in an overall accuracy of 89.14 % (Table 11). For the year 2019, the classification Kappa statistics value was 0.8643. The confusion matrix was calculated using Google Earth and KII to validate the accuracy for the years 1987 and 2003, yielding overall accuracy of 81.90 % and 83.81 %, respectively. For the years 1987 and 2003, the overall LULC classification Kappa statistics were 0.7829 and 0.8057, respectively.

Table 11: Confusion matrix of the year 2019 LULC supervised classification

Class name	1987		2003		2019	
	Producers Accuracy	Users Accuracy	Producers Accuracy	Users Accuracy	Producers Accuracy	Users Accuracy
FC	85.71%	96.77%	97.14%	94.44%	91.43%	96.97%
SET	71.43%	96.15%	94.29%	89.19%	88.57%	96.88%
SH	82.86%	61.70%	82.86%	96.67%	85.71%	90.91%
AG	91.43%	80.00%	91.43%	74.42%	91.43%	80.00%
WB	62.86%	95.65%	51.43%	94.74%	0	0
WE	97.14%	79.07%	85.71%	66.67%	88.57%	83.78%
Overall Accuracy	81.90%		83.81%		89.14%	
(K^)	0.7829		0.8057		0.8643	

Where: FC= Forest cover, SET= Settlement, SH= Shrub land, AG= Agriculture, WB= Water body and WE= Wetland.

3.4. Normalized difference vegetation index

In this study, it has been observed that the vegetation cover was very high in 1987 than in 2003 with maximum NDVI values of 0.61 and 0.48 respectively. This indicates that there was high healthy vegetation cover in 1987 than in 2003. Urban expansion and depletion of vegetation cover in 2003 were responsible for the decline of NDVI values. In 2019, vegetation cover was slightly increased and this made the NDVI value increase from 0.48 to 0.52 (Table 12).

As indicated in Figure 6 vegetation cover has decreased and the non-vegetated area has been increasing gradually over the study period. However, in 2019 plantation of (some trees and cash crops area has slightly increased due to the plantation program both in rural and urban areas). Settlement and agricultural land have low NDVI values. This is because of the dry nature of those

surfaces and their high thermal emittance property. So, this indicates that there was an indirect relationship between NDVI and LST. Sun *et al.,* (2012) and Yue *et al.,* (2007) revealed that LST has inversely related to NDVI.

Table 12: Normalized difference vegetation index results in 1987, 2003 and 2019

	1987				2003				2019			
Class			Mean				Mean				Mean	
Name	Min	Max	NDVI	STD	Min	Max	NDVI	STD	Min	Max	NDVI	STD
FC	0.13	0.61	0.39	0.05	0.09	0.48	0.32	0.05	0.01	0.52	0.29	0.06
SET	-0.07	0.46	0.21	0.07	-0.32	0.30	0.00	0.10	-0.42	0.40	0.18	0.06
SH	0.26	0.42	0.33	0.03	-0.01	0.37	0.16	0.06	0.10	0.44	0.30	0.04
AG	0.01	0.45	0.24	0.05	-0.33	0.36	0.01	0.09	-0.03	0.45	0.26	0.05
WB	-0.22	0.14	-0.08	0.09	-0.04	0.10	-0.12	0.12	0.00	0.00	0.00	0.00
WE	0.28	0.59	0.40	0.05	0.12	0.38	0.23	0.04	0.05	0.47	0.32	0.05

Where: FC= Forest cover, SET= Settlement, SH= Shrub land, AG= Agriculture, WB= Water body, WE= Wetland, MIN = Minimum, MAX = Maximum, STD = Standard deviation.

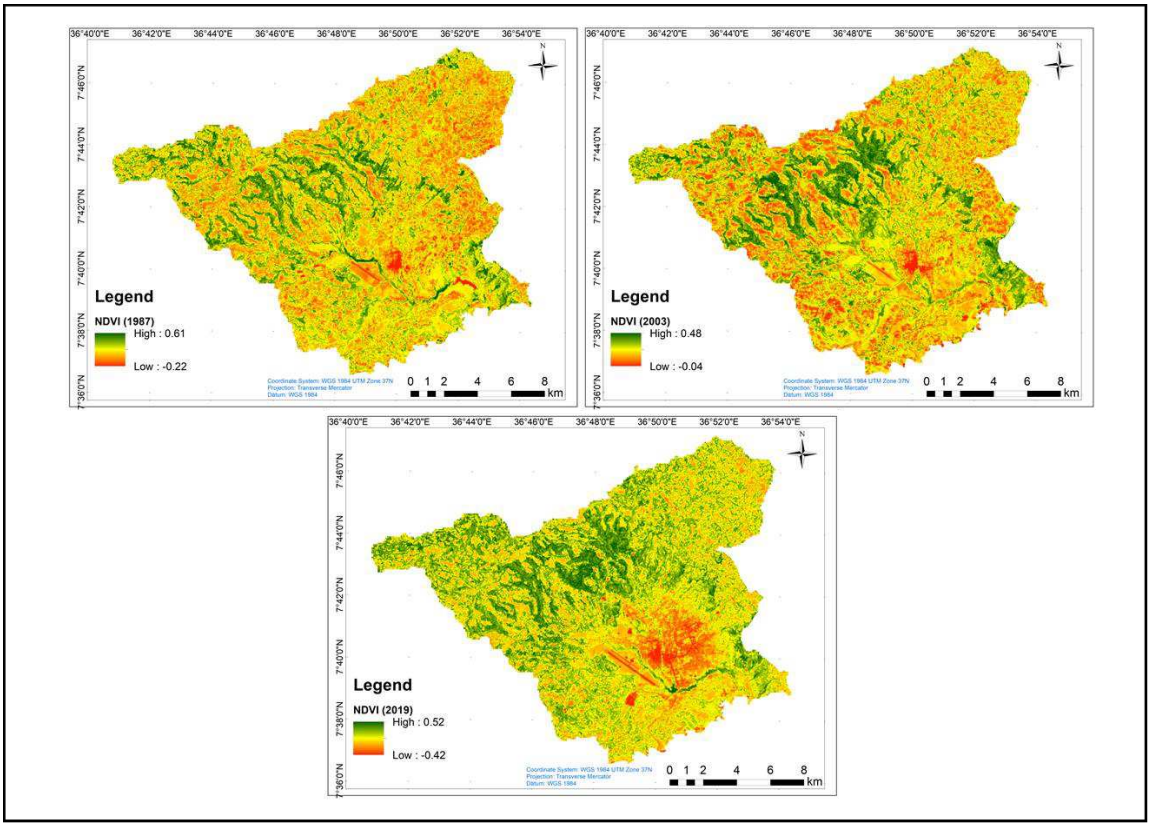

Figure 6: NDVI map of Jimma city and its surrounding in 1987, 2003 & 2019

3.5. Normalized difference built-up index

High NDBI values were concentrated around agricultural land and in the city area of Jimma. The build-up areas and bare land reflect more SWIR than NIR. In the case of a green surface, a reflection of NIR is higher than the SWIR spectrum (Zha *et al.,* 2003). Hence the lower value of NDBI represents vegetation whereas the higher value represents settlement and agricultural areas. In agreement with the finding of this research, a study conducted by Xiong *et al.,* (2012) found that high-temperature anomalies are closely associated with built-up land, densely populated zones, and heavily industrialized districts. Figure 7 indicated that the NDBI values were increased around Jimma city.

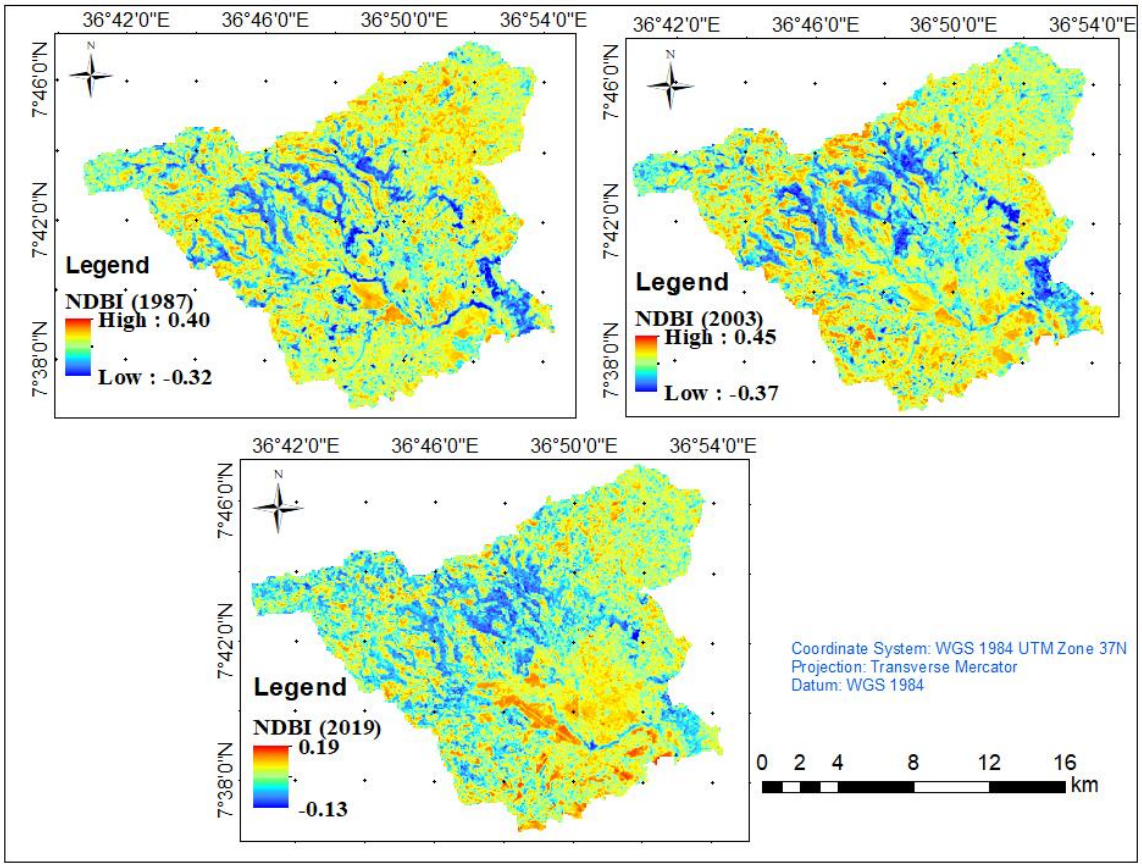

Figure 7: NDBI map of Jimma city and its surrounding in 1987, 2003 & 2019

3.6. The relationship of LST and LULC

Table 13 summarizes the LST and NDVI regressions for each LULC, with R^2 indicating the regression's determination coefficient. Forest cover, shrub land, and agricultural land had greater NDVI-to-LST coefficients. In wetland, water bodies, and settlement land, however, the LST and NDVI coefficients were small during the study period. Overall, the minimum temperature was found in the range of 12.36˚C in forest cover in 1987 to 21.53˚C in a settlement in 2019 while, the maximum temperature was recorded in the range of 19.28˚C in water body in 1987 to 33.68˚C in agricultural land in 2019 (Figure 8 and Table 14). In addition, the mean temperature was seen at around 16˚C in the water body in 1987 to 28˚C in the settlement in 2003. The lowest value for minimum 12.36˚C, maximum 19.28˚C, and mean 16.22˚C temperature can be found in the year 1987. Meanwhile, the highest value for the minimum temperature was occurred in 2019 (21.51˚C) in the settlement, and the highest value of the maximum and mean temperature was occurred in

2003 (35.92˚C and 28.16˚C) in a settlement. The lowest rate of increase in LST is found under forest cover.

Table 13: Linear regression equations between LST and LULC

years	LULC	Regression	R^2
1987	FC	LST = -7.3477x NDVI + 16.723	0.8919
	SET	LST = -0.2627x NDVI + 19.582	0.0001
	SH	LST = -13.858x NDVI + 23.007	0.1554
	AG	LST = -7.2137x NDVI + 22.259	0.0414
	WB	LST = -3.8903x NDVI + 15.705	0.0103
	WE	LST = -6.4279x NDVI + 21.188	0.0119
2003	FC	LST = -12.523x NDVI + 27.05	0.3129
	SET	LST = -1.6249x NDVI + 22.533	0.0049
	SH	LST = -12.685x NDVI + 28.318	0.2894
	AG	LST = -12.917x NDVI + 27.231	0.1941
	WB	LST = -1.3986x NDVI + 20.666	0.0256
	WE	LST = -13.969x NDVI + 27.883	0.1837
2019	FC	LST = -25.305x NDVI + 33.041	0.8043
	SET	LST = -20.946x NDVI + 30.51	0.335
	SH	LST = -20.519x NDVI + 31.032	0.4441
	AG	LST = -21.849x NDVI + 31.193	0.4342
	WB	- -	-
	WE	LST = -20.648x NDVI + 30.719	0.3618

Table 14: The mean LST and its standard deviation in different LULC types, which were calculated through GIS spatial partition statistics.

	1987				2003				2019			
Class Name	Min	Max	Mean LST	STD	Min	Max	Mean LST	STD	Min	Max	Mean LST	STD
FC	12.36	25.40	17.29	1.90	17.09	29.31	22.11	1.46	20.11	32.10	23.57	1.39
SET	13.78	27.51	20.53	1.83	17.62	35.92	28.16	2.12	21.51	33.60	26.79	1.64
SH	13.78	24.54	19.15	1.55	18.15	32.18	25.14	1.59	21.02	30.63	24.60	1.30
AG	13.78	26.67	19.59	1.84	16.55	34.99	26.85	2.23	21.03	33.68	25.82	1.63
WB	15.64	19.28	16.22	0.55	19.21	29.30	21.61	1.10	-	-	-	-
WE	14.25	24.11	17.50	1.65	20.26	32.18	24.68	1.43	21.02	32.29	25.04	1.56

Where: FC= Forest cover, SET= Settlement, SH= Shrub land, AG= Agriculture, WB= Water body, WE= Wetland, MIN = Minimum, MAX = Maximum, STD = Standard deviation.

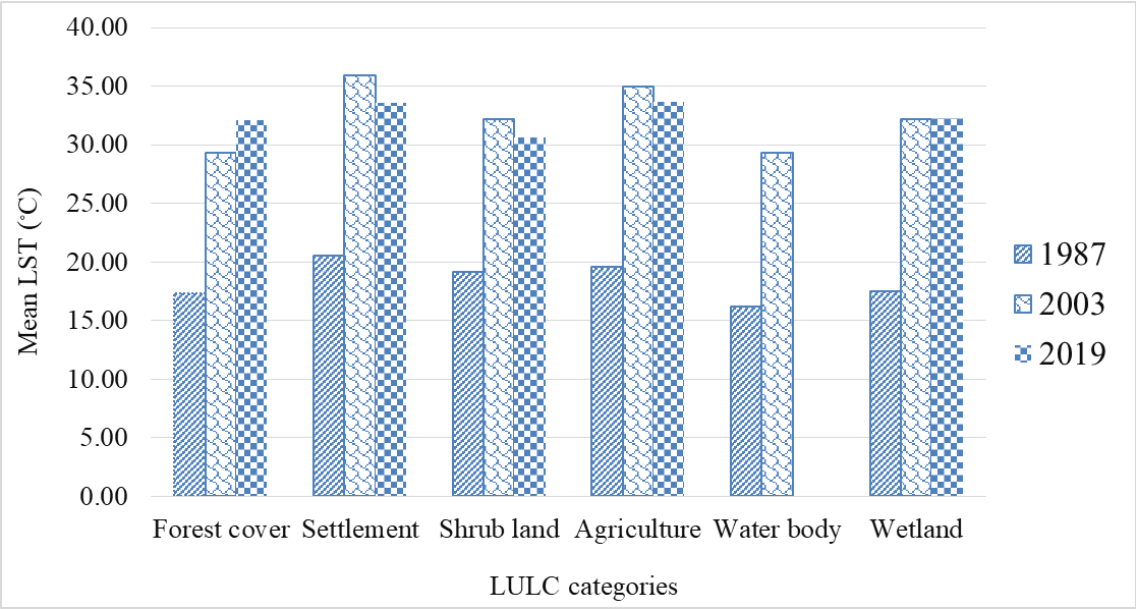

Figure 8: The mean LST in different LULC types.

To understand the relationship that exists between the land cover types and the LST, the mean value of the LST for 2019 and the corresponding percentage proportion of NDVI was investigated for each land cover type through correlation analysis (Table 15). The results show that there is a strong negative correlation between the mean LST and the percentage proportion of the vegetated areas of the Forest cover, shrub land, and wetland. This means that as the proportion of vegetated surfaces increases, the mean LST decreases. These results were found to be highly significant at $P < 0.01$. In contrast, other results revealed a strong positive correlation between the mean LST and percentage proportion of non-vegetated areas such as settlement and agricultural land implies that as the percentage proportion of non-vegetated areas increases, the mean LST increases. The results were also highly significant at $P < 0.01$. Because of this relationship between LST and NDVI, changes in LULC have an indirect impact on surface temperatures through NDVI. 1Ho is rejected and 1H1 is accepted based on the significant value of the p test results. This suggests that LULC has a significant impact on the temperature of the land surface.

Table 15: Pearson's correlations between LST and each indices of LULC 2019

Variables	LST	FC	SET	SH	AG	WE
LST	1	-.449**	.868**	-.660**	.674**	-.643**
FC	-.449**	1	.135	.268*	.235	.455*
SET	.868**	.135	1	-.632**	.305	-.682**
SH	-.660**	.268*	-.632**	1	.115	.393
AG	.674**	.235	.305	.115	1	-.164*
WE	-.643**	.455*	-.682**	.393	-.164*	1

**. Correlation is significant at the 0.01 level (2-tailed).

*. Correlation is significant at the 0.05 level (2-tailed).

Where: FC= Forest cover, SET= Settlement, SH= Shrub land, AG= Agriculture, WB= Water body and WE= Wetland.

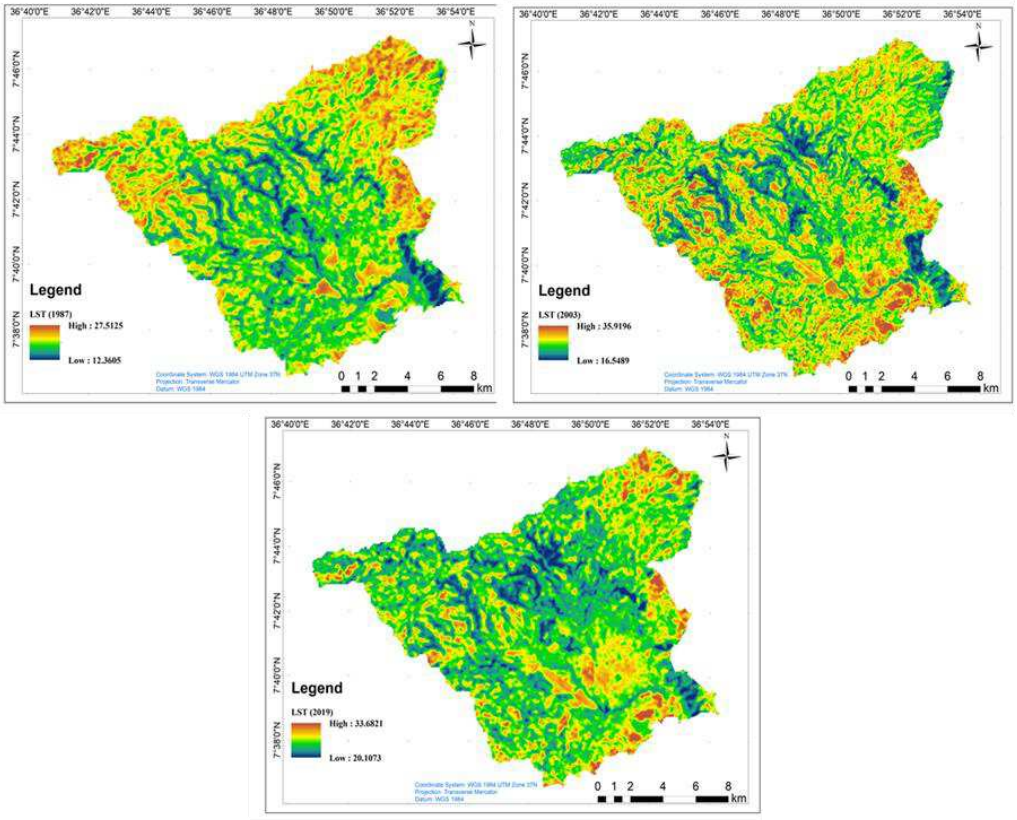

Figure 9: LST map of Jimma city and its surrounding in 1987, 2003 & 2019

Figure 9 and Table 14 shows that high surface temperature was observed in settlement land and agricultural land whereas the low surface temperature in green vegetative and wetland areas. Therefore, with the expansion of the vegetated area, the LST value adversely decreases and the expansion of non- evaporating surface brought an increase in LST. An increase in density of settlement, reduction in open space and green cover, increase in built-up space improves the LST of the urban area (Lilly & Devadas, 2009). With the rapid growth and expansion of the urban area, the propensity for the conversion of LULC into a built-up area and dwelling unit (non-evaporating surface) becomes high. Thus, such surfaces have a high probability of showing a greater value of LST.

Table 16: Model summary of LST and each indices of LULC 2019

Model	R	R Square	Adjusted R Square	Std. Error of the Estimate
1	.911[a]	.829	.749	.15960

a. Predictors: (Constant),

b. Dependent Variable:

For the full regression model, R^2 of 0.829 indicated the explanatory power of the model (Table 16). Thus, 82% of the variation in the dependent variables was explained by the regression. The significant value of 0.000 is lesser than the alpha value of 0.05, which indicates that the independent variables are statistically significant for the prediction of the dependent variable (Table 17), $F(7, 15) = 10.396$, $p < 0.05$ which means the adopted regression model is a good fit of the data.

Table 17: ANOVA of LST and each indices of LULC 2019

Model		Sum of Squares	df	Mean Square	F	Sig.
1	Regression	1.854	7	.265	10.396	.000[b]
	Residual	.382	15	.025		
	Total	2.236	22			

a. Dependent Variable: LST_2019

b. Predictors: (Constant),

From Figure 10 Forest cover type was located in the right lower corner of the diagram, shrub land, and wetland areas were located in the center of the diagram (medium values for both parameters, NDVI and LST), while the settlement and agricultural land areas were located at the upper left corner of the diagram. In other words: the NDVI confirms the cluster structure of land cover types derived from surface temperatures

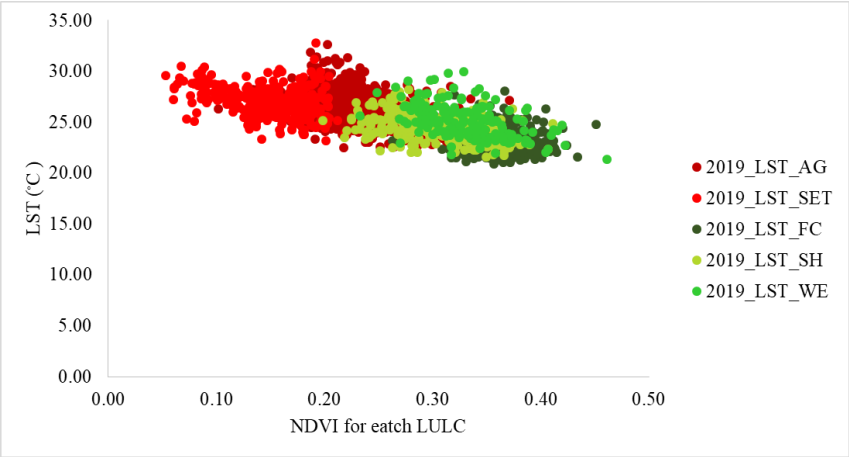

Figure 10: Scatterplot of LST vs. NDVI (2019).

3.7. Multiple correlation matrix analysis of LST, NDVI, and NDBI

The analyzed Landsat images of 1987 and 2019 indicated that LST had a positive relationship with NDBI and an inverse relationship with NDVI.

Table 18: Model Summary of LST and NDVI and NDBI for 1987, 2003 & 2019

Years	Model	R	R Square	Adjusted R Square	Std. Error of the Estimate
1987	1	.831[a]	.691	.689	1.26820
2003	1	.880[a]	.774	.773	1.34958
2019	1	.885[a]	.784	.782	1.05233

a. Predictors: (Constant), NDBI, NDVI

From the processing results obtained summary (Table 18) which shows the values of determination (R^2) to determine the percentage contribution of the influence of the independent variables to the dependent variable and the values of R (multiple correlation coefficients) which are considered as a measure of the worth of the prediction of the dependent variables. The R-value of 0.831, 0.880, and 0.885 for the years 1987, 2003, and 2019 respectively indicate a good level of prediction. The

coefficient of determination was represented by R^2 which shows the proportion of variance in the dependent variable that can be explained by the independent variables. The R square values were 0.691, 0.774, and 0.784 for the years 1987, 2003, and 2019 respectively; therefore, above 69.1%, 77.4%, and 78.4% of the variation in the land surface temperature (dependent variable) was explained by NDVI and NDBI (independent variables) shown in Table 18.

Simultaneously it can be seen from the F-ratio in the ANOVA test results. (Table 19) shows that the independent variables highly statistically significantly predict the dependent variable, F (2, 366) =326.166, p (0.000), (2, 366) =416.379, p (0.000) and (2, 366) =238.771, p (0.000) for the year 1987, 2003 and 2019 respectively (i.e., the regression model is a good fit of the data). Table 19 shows the analysis of variance, which shows the overall regression model is a good fit for the given data.

Table 19: ANOVA of LST and NDVI and NDBI for 1987, 2003 & 2019

year	Model		Sum of Squares	df	Mean Square	F	Sig.
1987	1	Regression	1049.170	2	524.585	326.166	.000[b]
		Residual	468.652	366	1.608		
		Total	1517.822	368			
2003	1	Regression	1247.080	2	623.540	416.379	.000[b]
		Residual	448.096	366	1.498		
		Total	1695.176	368			
2019	1	Regression	745.220	2	282.610	238.771	.000[b]
		Residual	253.199	366	1.184		
		Total	998.419	368			

a. Dependent Variable: LST

b. Predictors: (Constant), NDBI, NDVI

Table 20 and Figures 11a-c show the unstandardized coefficient (B), which tells the relationship between the land surface temperature and other independent variables. There was a strong negative correlation (B = -0.078) between LST and NDVI of the year 1987 and highly statistically significant ($\rho = 0.000$). NDVI of the year 2003 shows a negative correlation (B = -0.048) with LST and is statistically significant ($\rho = 0.000$). There was also a strong negative correlation (B= -0.022)

between LST and NDVI of the year 2019 and statistically significant (ρ= 0.000). Malik *et al.,* (2019), Balew (2018), and Haylemariya (2018) revealed that LST has inversely related to NDVI. The negative value of NDVI implies that the land surface temperature increase, with decreases in vegetation, so LST is negatively related to NDVI. According to KII, Jimma city's forest cover has been converted to built-up other infrastructure. Other LULC, such as wetland, shrub land, and forest land, were also converted to agricultural land and settlement. Transformation of vegetation areas, expansion of settlement land, and agricultural land were responsible for the increase of LST in the study area. If the deforestation and cut of urban trees are not stopped, then this situation will continue to be worse day by day.

Table 20: Coefficients of LST and NDVI and NDBI for 1987, 2003 & 2019

year	Model		Unstandardized Coefficients		Standardized Coefficients			95.0% Confidence Interval for B	
			B	Std. Error	Beta	t	Sig.	Lower Bound	Upper Bound
1987	1	(Constant)	19.641	.659		29.796	.000	18.345	20.937
		NDVI	-.078	1.793	-.025	-3.741	.000	-10.234	-3.182
		NDBI	.572	1.519	.038	7.618	.000	8.586	14.558
2003	1	(Constant)	25.267	.369		68.546	.000	24.542	25.991
		NDVI	-.048	1.371	-.036	-5.459	.000	-10.176	-4.787
		NDBI	.612	1.165	.060	9.970	.000	9.321	13.902
2019	1	(Constant)	28.933	.390		74.097	.000	28.165	29.701
		NDVI	-.022	1.718	-.001	-5.880	.000	-13.481	-6.724
		NDBI	.759	1.340	.049	8.337	.000	8.534	13.802
	a. Dependent Variable: LST								

The linear regression between LST and NDBI and the trend analysis in Figure12a-c and Table 20 represents the rise of LST with the increase of NDBI value over time. The value of the coefficient of determination, R^2= 0.754 in 1987 (Figure12a) describes the strong responsive relationship between LST and NDBI. The transformation of other land cover types in buildup areas has influenced the relationship in the year 2019. The value of R^2= 0.739 in the year 2019 (Figure 12c) indicates the strongly significant positive relationship between LST and NDBI. The coefficient of determination in Figures 12a, b, c suggests that the increase of settlement area is responsible for the increase of surface temperature in the study area during the study period. NDBI was strongly

positively correlated (B = 0. 572, B= 0.612 and B= 0.759) to the LST and indicate highly statistically significant (ρ = 0.000) for the year 1987, 2003 and 2019 respectively. The positive B value of NDBI indicates that an increase in settlement land will increase the temperature which indicates that LST is positively related to NDBI.

Table 20 also show 1987 NDVI (t = -3.741, p < 0.05), 1987 NDBI (t = 9.970, p < 0.05), 2003 NDVI (t = -5.459, p < 0.05), 2003 NDBI (t = 7.618, p < 0.05), 2019 NDVI (t = -5.880, p < 0.05), 2019 NDBI (t = 8.337, p < 0.05) are significant predictors of land surface temperature.

Based on the results of the t-test, the significance value of each variable was less than 0.05 then the hypothesis 2H1 was accepted. Therefore, the NDVI and the NDBI both have a significant effect on the surface temperature of Jimma city and its surrounding. From the magnitude of the t-statistics, the expansion of settlement land had more impact on the LST confirmed by standardized coefficients.

The model also tells that with one unit increase in the vegetation, the temperature would decrease by 0.078, 0.048, and 0.022 units for the years 1987, 2003, and 2019 respectively; similarly, with one unit increase in the settlement land, there would be an increase of 0.612, 0.572 and 0.759 units in the LST for the year 1987, 2003 and 2019 respectively.

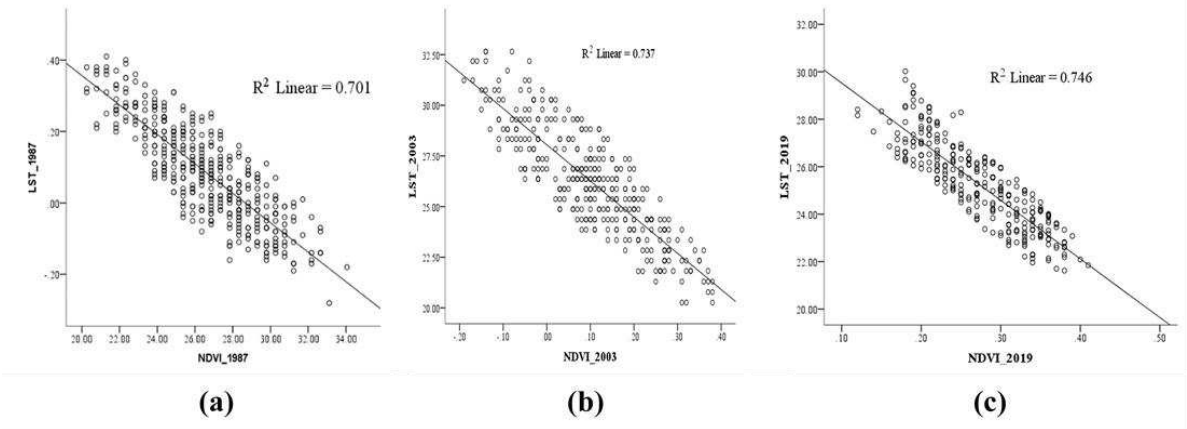

Figure 11: linear correlation between LST in response to NDVI in the year (a) 1987, (b) 2003, and (c) 2019.

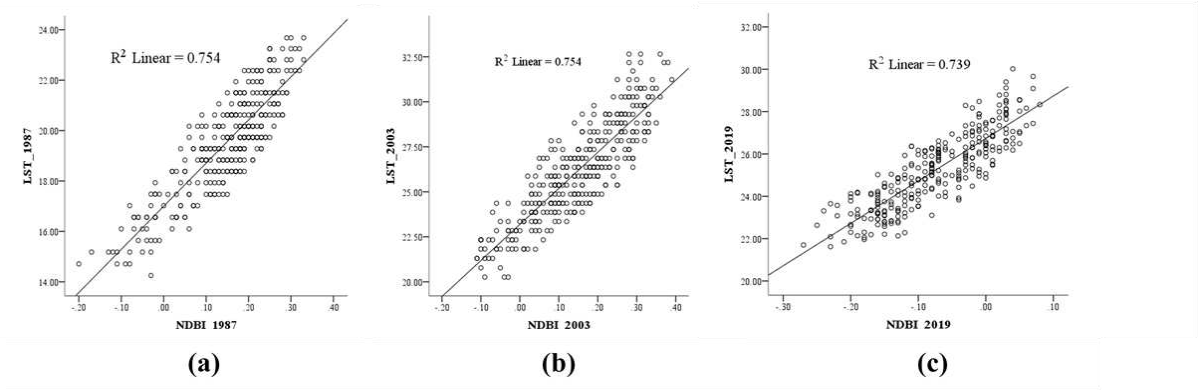

Figure 12: linear correlation between LST in response to NDBI in the year (a) 1987, (b) 2003, and (c) 2019.

The relationship between NDVI and NBDI has also been developed during the study. NDVI has shown a strong negative correlation with NDBI in each year i.e. $R^2 = 0.739$ in 1987 0.860 in 2003 and 0.801 in 2019. The linear correlation of NDVI vs. NDBI is displaying in the scatter plot (Figure. 13a-c).

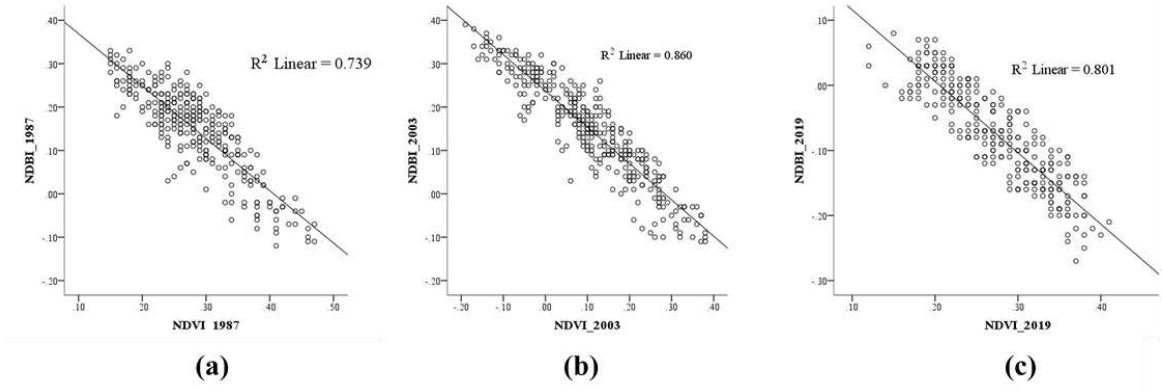

Figure 13: linear correlation between NDBI in response to NDVI in the year (a) 1987, (b) 2003, and (c) 2019.

4. Conclusion and Recommendations

4.1. Conclusion

The results of this study revealed that there was a shift in LULC during the course of the study period. The proportion of land used for settlement and agricultural purposes has been steadily rising. Waterbody, shrubland, wetland, and forest cover, on the other hand, have been declining. As a result, there were more open spaces and deforestation, resulting in a rise in LST. The lowest

LST was found in areas with forest land, waterbody, wetland, and shrubland, while the greatest LST was found in areas with settlement land and agricultural land. The developed correlation of LST with NDBI and NDVI has shown $R^2 = 0.691$ in 1987, 0.774 in 2003, & 0.784 in 2019. Strong negative correlation resulted between NDVI & NDBI i.e. $R^2 = 0.739$ in 1987, 0.860 in 2003, & 0.801 in 2019, respectively. LST and NDBI have a significant positive correlation, implying that as settlement land and open land increase, so does land surface temperature. The significant negative relationship between NDVI and LST suggests that healthy green vegetation reduces surface temperature. Thus, future LST study may be collected at multiple geographical resolutions and during different seasons of the year to analyze the LST, with additional parameters like soil moisture, water bodies, and population density being utilized to determine their influence on LST. Accelerating afforestation and reforestation initiatives, as well as maintaining naturally regenerated trees, should be prioritized.

Abbreviations

LTS stands for land surface temperature; NDVI stands for normalized difference vegetation index; NDBI stands for normalized difference built-up index; LSE stands for land surface emissivity; WORMC stands for Western Oromia region meteorological center; ERDAS stands for Earth Resource Data Analysis System; LULC stands for land use land cover; LULCC stands for land use land cover change; USGS stands for United States Geological Survey; TM stands for Thematic Mapper; ETM+ stands for Enhanced Thematic Mapper; OLI/TIRS stands for operational land imager/thermal infrared sensor; GIS stands for Geographic Information System; GPS stands for Global Positioning System, EROS stands for Earth Resources Observation and Science, MLC stands for Maximum Likelihood Classification, OA stands for Overall accuracy

Ethics approval and consent to participate

Not applicable.

Materials and data availability

The three Landsat images were obtained from the United States Geological Survey's Center for Earth Resources Observation and Science (EROS). Fieldwork and in-depth discussions with local elders, who were chosen from the local community and agricultural development agents, were also used to collect primary data.

Consent for publication

I have agreed to submit for Environmental Systems Research and approved the manuscript for submission.

Competing interests

Not compete for interest.

Funding

The study was not funded by any organization

Acknowledgement

I would like to extend my deepest gratitude, first and foremost, to God, who creates this world in his word and help us in all aspects of our life.

Authors' contributions

Nigus Tekleselassie Tsegaye prepared the original version of the manuscript and Girma Alemu revised and edited the paper

References

Aadil, M., Rafiq, A., Aadil, H. & Pervez, A., 2014. Changes in land-use/land-cover dynamics using geospatial techniques: A case study of Vishav drainage basin. *J. Geogr. Reg. Plan.,* 7, pp. 69–77.

Abebe, M. S., Derebew, K. T. & Gemeda, D. O., 2019. Exploiting temporal-spatial patterns of informal settlements using GIS and remote sensing technique: a case study of Jimma city, Southwestern Ethiopia. *Environ Syst Res,* 8(6).

Abrha, C., Feyisa, G. L. & Feyssa, D. H., 2015 . Analysis of land use/cover dynamics in Jimma city, Southwest Ethiopia: an application of satellite remote sensing. *Ethiop.J.Appl.Sci. Technol.,* 6(2), pp. 24-34.

Ali-Toudert, F. & Mayer, H., 2007. Effects of asymmetry, galleries, overhanging facades and vegetation on thermal comfort in urban street canyons. *Sol. Energy,* 81, pp. 742-754.

Alqurashi, A. & Kumar, L., 2013. Investigating the Use of Remote Sensing and GIS Techniques to Detect Land Use and Land Cover Change: A Review. *Advances in Remote Sensing,* 2, pp. 193-204 .

Alshaikh, A., 2015.Vegetation cover density and land surface temperature interrelationship using satellite data, case study of Wadi Bisha, South KSA. *Advances in Remote Sensing,* 4, pp. 248-262.

Amiri, R., Weng, Q., Alimohammadi, A. & Alavipanah, S., 2009. Spatial–temporal dynamics of land surface temperature in relation to fractional vegetation cover and land use/cover in the Tabriz urban area, Iran. *Remote Sens. Environ.,* 113, pp. 2606-2617.

Arvor, D., Dubreuil, V., Simões, M. & Bégué, A., 2014. Mapping and spatial analysis of the soybean agricultural frontier in Mato Grosso, Brazil, using remote sensing data. *GeoJournal,* 78, pp. 833–850.

Balew, A., 2018. Impacts of Land-Use and Land-Cover Changes on Land Surface Temperature Distribution in Bahir Dar Town and Its Surroundings Using Remote Sensing. Msc thesis.

Chen, D., Wang, X., Khoo, Y.B., Thatcher, M., Lin, B.B., Ren, Z., Barnett, G., 2013. Assessment of urban heat island and mitigation by urban green coverage. *In Mitigating climate change (Springer Berlin Heidelberg),* pp. 247-257.

Congalton, R., 1991. A review of assessing the accuracy of classifications of remotely sensed data. *Remote Sensing of Environment,* 37(1), pp. 35-46.

Coskun, H. G., Alganci, U. &Usta,G.,2008.Analysis of Land Use Change and Urbanization in the Kucukcekmece Water Basin (Istanbul, Turkey) with Temporal Satellite Data using Remote Sensing and GIS. *Sensors,* 8, pp. 7213-7223.

Deribew, K. T. & Dalacho, D. W., 2019. Land use and forest cover dynamics in the North-eastern Addis Ababa, central highlands of Ethiopia. *Environ Syst Res ,* 8(8), pp. 1-18.

Dube, E. E., 2013 . Urban planning and land management challenges in emerging towns of Ethiopia: the case of Arba Minch. *Journal of Urban and Environmental Engineering ,* 7(2), pp. 340-348.

Farooq, A., Qurat-ul-ain, F., Hir, J.B., Kashi, S., Sajid, R.A. & Shafeeq-Ur, R., 2013. *Glob J Hum Soc Sci ,* 13, pp. 21–42.

Gao, J., 2009. Digital Analysis of Remotely Sensed Imagery. McGraw-Hill.

Garai, D. & Narayana, A., 2018. Land use/land cover changes in the mining area of Godavari coal fields of southern India. *EJRS,* 21, pp. 375-381.

Grover, A. & Singh, R., 2015. Analysis of urban heat island (UHI) in relation to normalized difference vegetation index (NDVI): A comparative study of Delhi and Mumbai.. *Environ.,* 2, pp. 125-138.

Haylemariyam, M. B., 2018. Detection of Land Surface Temperature in Relation to Land Use Land Cover Change: Dire Dawa City, Ethiopia. *Journal of Remote Sensing & GIS,* 7(3).

Hu, Y. & Jia, G., 2010. Influence of land use change on urban heat island derived from multi-sensor data.,. *Int. J. Climato.,* 30, pp. 1382-1395 .

Igun, E. & Williams, M., 2018. Impact of urban land cover change on land surface temperature. *Global J. Environ. Sci. Manage.,* 4(1), pp. 47-58.

Lilly R., A. & Devadas, M., 2009. Analysis of land surface temperature and land use/land cover types using remote sensing imagery-a case in Chennai city, India. *In The seventh International Conference on Urban Climate.*

Liu, L. & Zhang, Y., 2011. Urban heat island analysis using the Landsat TM data and ASTER data: A case study in Hong Kong. *Remote Sens.,* 3, pp. 1535–1552.

Mahmood, R. R., A., Pielke, SR.R., kenneth, G., Hubbard, niyogi, D., Gordon, B.; Peter, L., Richard, Mc., Clive, Mc., Andres, E., Samuel, G.& Budong, Q., 2010. Impacts of land use/land cover change on climate and future research priorities. *Bulletin of the American Meteorological Society,* 91, pp. 37-46.

Malik, M., Shukla, J. & Mishra, S., 2019. Relationship of LST, NDBI and NDVI using Landsat-8 data in Kandaihimmat Watershed, Hoshangabad, India. *Indian Journal of Geo Marine Sciences,* 48(01), pp. 25-31 .

Meijun, J., Junming, L., Caili, W. & Ruilan, S., 2015. A Practical Split-Window Algorithm for Retrieving Land Surface Temperature from Landsat-8 Data and a Case Study of an Urban Area in China. *Remote Sens.,* 7, pp. 4371–4390.

Mosammam, H.M., Nia, J.T., Khani, H., Teymouri, A.& Kazemi, M., 2017. Monitoring land use change and measuring urban sprawl based on its spatial forms. The case of Qom city. *Egypt J Rem Sens Space Sci.,* 20, pp. 103–116.

NASA, 2000. Landsat 7 Science Data Users Handbook.

Onishi, A., Cao, X., Ito, T., Shi, F.& Imura, H., 2010. Evaluating the potential for urban heat-island mitigation by greening parking lots. *Urban For Urban Greening,* 9, pp. 323-332.

Orimoloye, I., Mazinyo, S., Nel, W. & Kalumba, A., 2018. Spatiotemporal monitoring of land surface temperature and estimated radiation using remote sensing: human health implications for East London, South Africa. *Environ. Earth Sci.,* 77(77), pp. doi:10.1007/s12665-018-7252-6.

Polydoros, A., Mavrakou, T. & Cartalis, C., 2018. Quantifying the Trends in Land Surface Temperature and Surface Urban Heat Island Intensity in Mediterranean Cities in View of Smart Urbanization. *Urban Science,* 2(1), pp. 16.

Pongratz, J., Reick, C. H., Raddatz, T. & Claussen, M., 2010. Biogeophysical versus biogeochemical climate response to historical anthropogenic land cover change Geophys. *Res. Lett.,* 37 (16), pp. 2–9.

Rajeshwari, A. & Mani, N. D., 2014. Estimation of land surface temperature of Dindigul Woreda using Landsat 8 data. *International Journal of Research in Engineering and Technology,* 3(5), pp. 122–126.

Raynolds, M., Comiso, J., Walker, D. & Verbyla, D., 2008. Relationship between satellite-derived land surface temperatures, arctic vegetation types, and NDVI. *Remote Sens. Environ.,* 112, pp. 1884-1894.

Richards, J. & Jia, X., 2006. *Remote Sensing Digital Image Analysis: An introduction.* 4th ed. Germany: Springer-Verlag Berlin Heidelberg 2006.

Roberts, D.A., Dennison, P.E., Roth, K.L., Dudley, K.& Hulley, G., 2015. Relationships between dominant plant species, fractional cover and Land Surface Temperature in a Mediterranean ecosystem. *Remote Sensing of Environment,* 167, pp. 152-167, (https://doi.org/10.1016/j.rse.2015.01.026).

Rotem-Mindali, O., Michael, Y., Helman, D. & Lensky, I. M., 2015. The role of local land-use on the urban heat island effect of Tel Aviv as assessed from satellite remote sensing. *Appl. Geogr.,* 56, pp. 145-153.

Russell, G., Congalton & Kass, G., 2019. *Assessing the Accuracy of Remotely Sensed Data: Principles and Practices.*3rd ed. Inc., Boca Raton, London, New York, Washington DC: CRC press.

Sahana, M., Ahmed, R. & Sajjad, H., 2016. Analyzing land surface temperature distribution in response to land use/land cover change using split-window algorithm and spectral radiance model in Sundarban Biosphere Reserve, India. *Modeling Earth Systems and Environment,* 2, pp. 81.

Sahoo, S., 2013. Monitoring urban Land use land cover change by multi-temporal remote sensing information in Howrah City, India. *Int. Res. J. Earth Sci.,* 1(5), pp. 1–6.

Sun, Q., Wu, Z. & Tan, J., 2012. The relationship between land surface temperature and land use/land cover in Guangzhou, China. *Environ. Earth Sci.,* 65, pp. 1687–1694.

UN, 2014. World Urbanization Prospects: The 2014 Revision, Highlights (No. ST/ESA/SER.A/352). United Nations, Department of Economic and Social Affairs, Population Division, New York.

UN-HABITAT, 2010. State of the World's Cities 2010/2011: Prosperity of Cities. Earthscan, UK, United Nations Human Settlements Programme.

USGS, 2019. *Landsat 8 (L8) Data Users Handbook.*. 5 ed. s.l.:Department of the Interior U.S. Geological Survey.

Veldkamp, A. & Lambin, E., 2001. Predicting land-use change. *Agric. Ecosyst. Environ.,* Volume 85, pp. 1-6.

Weng, Q. & Lu, D., 2008. A sub-pixel analysis of urbanization effect on land surface temperature and its interplay with impervious surface and vegetation coverage in Indianapolis, United States. *Int. J. Appl. Earth Obs. Geoinf.,* 10, pp. 68-83.

Weng, Q., Lu, D. & Schubring, J., 2004. Estimation of land surface temperature–vegetation abundance relationship for urban heat island studies. *Remote Sens. Environ.,* 89, pp. 467-483.

Western Oromia region Meteorology Center, 2019. *Jimma Town Rain fall and tempreture distribution.,* Jimma: unpublished data.

Wim, H., Ambro, S. M. & Ben, G. H. G., 2004. *Principles of Remote Sensing: An introductory textbook.* 3rd ed. Netherlands: The International Institute for Geo-Information Science and Earth Observation (ITC), Hengelosestraat 99.

Xiong, Y., Huang, S., Chen, F., Ye, H., Wang, C.& Zhu, C., 2012. The impacts of rapid urbanization on the thermal environment: a remote sensing study of Guangzhou, South China. *Remote Sens.,* 4, pp. 2033–2056.

Yue, W., Xu, J., Tan, W. & Xu, L., 2007. The relationship between land surface temperature and NDVI with remote sensing: application to Shanghai Landsat 7 ETM+ dat. *Int. J. Remote Sens.,* 28, pp. 3205–3226.

Zengin, H., Degermenci, A. & Bettinger, P., 2018. Analysis of tempAnalysis of temporal changes in land cover and landscape metrics of a managed forest in the West Black Sea region of Northern Turkey: 1970–2010. *J. For. Res.,* 29, pp. 139-150.

Zha, Y., Gao, J. & S., N., 2003. Use of normalized difference built-up index in automatically mapping urban areas from TM imagery. *International Journal of Remote Sensing,* 24(3), pp. 583-594.

Zhibin, R., Haifeng, Z., Xingyuan, H., Dan, Z.& Xingyang, Y., 2015. Estimation of the relationship between urban vegetation configuration and land surface temperature with remote sensing. *J. Indian Soc. Remote Sens.,* 43, pp. 89-100 .